Mutations in Auxilin cause parkinsonism via impaired clathrin-mediated trafficking at the Golgi apparatus and synapse

Dorien A. Roosen[1, 2], Natalie Landeck[1], Melissa Conti[1], Nathan Smith[1, 3], Sara Saez-Atienzar[4], Jinhui Ding[5], Aleksandra Beilina[1] Ravindran Kumaran[1] Alice Kaganovich[1] Johann du Hoffmann[6] Chad D. Williamson[7] David C. Gershlick[8] Luis Bonet-Ponce[1] Luciana Sampieri[7] Christopher K. E. Bleck[9] Chengyu Liu[10] Juan S. Bonifacino[7] Yan Li[11] Patrick A. Lewis[2, 12] Mark R. Cookson[1, *]

1 Cell Biology and Gene Expression Section, Laboratory of Neurogenetics, National Institute on Aging, 35 Convent Drive, Bethesda, Maryland, USA

2 School of Pharmacy, University of Reading, Whiteknights Campus, Reading, UK

3 University of Nebraska-Lincoln, Department of Biochemistry, Redox Biology Center, Lincoln, Nebraska, USA

4 Neuromuscular Diseases Research Unit, Laboratory of Neurogenetics, National Institute on Aging, 35 Convent Drive, Bethesda, Maryland, USA

5 Computational Biology Group, Laboratory of Neurogenetics, National Institute on Aging, 35 Convent Drive, Bethesda, Maryland, USA

6 Rodent Behavioral Core, National Institute of Mental Health, 35 Convent Drive, Bethesda, Maryland, USA

7 Neurosciences and Cellular and Structural Biology Division, Eunice Kennedy Shriver National Institute of Child Health and Human Development, 35 Convent Drive, Bethesda, Maryland, USA

8 Cambridge Institute for Medical Research, University of Cambridge, Cambridge, UK

9 Electron Microscopy Core Facility, National Heart, Lung and Blood Institute, National Institutes of Health, Bethesda, Maryland, USA

10 Transgenic Core, National Heart, Lung and Blood Institute, National Institutes of Health, Bethesda, Maryland, USA

11 Proteomics Core, National Institute of Neurological Disorders and Stroke, 35 Convent Drive, Bethesda, Maryland, USA

12 Department of Molecular Neuroscience, UCL Institute of Neurology, London, UK

***** Corresponding author: Phone: +13014513870, Fax: +13014517295, Email: cookson@mail.nih.gov

Submitted: 5 November 2019

Abstract

Parkinson's disease (PD) is a common neurodegenerative motor disorder characterized in part by neuropathological lesions in the nigrostriatal pathway. While most cases of PD are sporadic in nature, several inherited monogenic syndromes exist that overlap clinically and pathologically with sporadic PD. Of these, loss of function mutations in *DNAJC6*, which encodes the protein Auxilin, cause an aggressive form of juvenile onset PD. Auxilin and its homologues are known to play a role in clathrin-mediated trafficking, which is crucial for cellular function in all eukaryotes and plays a specialized role in synaptic transmission in higher organisms. Auxilin is the major neuronal uncoating protein for clathrin-coated vesicles required for delivery of cargo from the plasma membrane and *trans*-Golgi network to intracellular destinations. However, how mutations in Auxilin cause PD is currently not understood. To address this problem, we generated a novel mouse model carrying an endogenous pathogenic Auxilin mutation. When bred to homozygosity, this mutation induced neurological phenotypes that phenocopy clinical features observed in patients, including motor impairments reminiscent of bradykinesia and gait problems. Mapping the interactome of Auxilin confirmed clathrin and synaptic clathrin adaptor protein interactions and also identified novel Golgi-resident interactors. Critically, all tested pathogenic mutations in Auxilin retained clathrin adaptor protein binding but lost interaction with clathrin itself. These observations describe a mechanism by which impaired clathrin-mediated trafficking in R857G Auxilin mice, both at the Golgi and the synapse, results in neuropathological lesions in the nigrostriatal pathway. Collectively, these results provide novel insights for PD pathogenesis in Auxilin mutation carriers, reinforcing a key role for clathrin-mediated trafficking in PD, and expand our understanding of the cellular function of Auxilin.

Keywords: Auxilin, GAK, parkinsonism, GGA2, Golgi, synapse, clathrin coated vesicles

Highlights

- Auxilin interacts with Golgi-resident clathrin adaptor protein GGA2
- Auxilin is involved with uncoating of CCVs at the Golgi and synapse
- Impaired clathrin-mediated trafficking underlies PD-like phenotypes in R857G Auxilin mice

Introduction

Parkinson's disease (PD) is a multisystem neurodegenerative disorder characterized by a range of motor and non-motor neurological symptoms, including the clinically diagnostic triad of bradykinesia, rigidity and tremor [1]. Although the neurochemical basis of PD has been understood for many decades, the underlying mechanisms driving the loss of neurons in the central nervous system of people with this disorder have remained, for the most part, obscure [2]. This gap in our knowledge has contributed to the absence of disease modifying therapies for PD.

The majority of PD cases are idiopathic in nature, however an estimated 5-10% of PD cases are inherited in a Mendelian fashion [3]. Investigations into the function and dysfunction of genes identified in Mendelian PD have provided important insights into the etiology of PD, highlighting protein aggregation, disruption of lysosomal biology, and mitochondrial quality control as key elements of the cellular events that lead to neurodegeneration [2, 4].

Mutations in *DNAJC6*, encoding the protein Auxilin, were first described in a series of young and juvenile onset patients with parkinsonism in 2012. The majority of these mutations are splice site mutations resulting in decreased Auxilin levels [3, 5] or nonsense mutations resulting in a C-terminal truncation of Auxilin [6, 7]. Alongside the autosomal recessive (AR) mode of inheritance, these mutations suggest a loss of function mechanism for disease, although one coding mutation has also been reported (R927G) [5]. The clinical phenotype associated with mutations in Auxilin is complex, with developmental delay, pyramidal symptoms and in some cases seizures in addition to a parkinsonian presentation [3, 5–7].

Auxilin is involved in the uncoating and release of clathrin-coated vesicles (CCVs) through co-ordination of HSC70 chaperone activity and by interacting with a panel of adaptor proteins (APs) [8–16]. Clathrin plays a central role in a number of cellular vesicle pathways, forming a cage-like structure and facilitating endocytosis and trafficking along the secretory pathway. Hence, Auxilin mutations implicate clathrin-mediated trafficking in PD pathogenesis. In humans, Auxilin is expressed exclusively in the central nervous system, with its close paralog G-Cyclin Associated Kinase (GAK), showing ubiquitous expression [17, 18]. Notably, *GAK* has been implicated in idiopathic PD through genome wide association studies and protein interactome analyses, suggesting that both Auxilin and GAK have a conserved role in the survival of dopaminergic neurons in the human brain [19–21]. The precise details of the mechanisms linking Auxilin to neurodegeneration have, however, yet to be elucidated.

Here, we set out to test the impact of coding variation in the *DNAJC6* gene causative for PD. We generated a new engineered rodent model to examine the organismal impact of the R927G mutation, in parallel with protein interactome analyses to shed light on the molecular basis for Auxilin dysfunction in PD. Our results provide the first evidence for neuronal dysfunction in a murine model for Auxilin mutations and demonstrate a novel role for Auxilin in the regulation and trafficking of CCVs derived from the *trans*-Golgi network (TGN). We show mechanistically that mutations in Auxilin are loss of function through diminished interaction with clathrin even though interactions with clathrin adaptor proteins were retained. These data reveal important insights that expand the landscape of vesicle trafficking defects linked to PD, opening up novel pathways that are relevant for therapeutic development in this disorder, as well as illuminating the basic function and biology of Auxilin in CCV activity.

Results

Pathogenic R857G Auxilin allele is hypomorphic during early development

To analyze the impact of the human pathogenic R927G Auxilin mutation at the physiological level *in vivo*, we developed a homozygous knockin (KI) mouse model carrying the equivalent endogenous homozygous murine variant R857G (Figure 1A, B; Figure S1). Analysis of Auxilin RNA expression in wild type (WT) mice confirmed expression in dopaminergic neurons in the nigrostriatal pathway, a major area impacted during PD pathogenesis (Figure 1C).

Analysis of Auxilin protein levels in primary neurons derived from newborn (p0) R857G Auxilin mice revealed lower Auxilin protein expression compared to WT controls (Figure 1D, E). Similarly, brain lysates of p0 as well as p2 R857G Auxilin mice had lower Auxilin protein levels than WT animals, with some variation between animals (Figure S2A, B, D, E). However, no differences in Auxilin protein levels were observed in the brain of p6 or 3 week old mice, indicating an age-dependent upregulation of Auxilin during early development of R857G Auxilin mice (Figure S2G, J). GAK, the ubiquitously expressed paralogue of Auxilin, has previously been found to be upregulated in the brain of Auxilin KO mice to compensate for the complete loss Auxilin function [22] and hence GAK protein levels in the brain of R857G Auxilin mice were analyzed. Only a modest, transient upregulation of GAK protein was observed in the brain of p2 R857G Auxilin mice (Figure S2D, F). Similar to conventional Auxilin KO mice [22], R857G Auxilin mice displayed increased perinatal mortality, as indicated by a deviation from the expected 1:2:1 inheritance from heterozygous breeding pairs 3 weeks after birth (Figure 1F). Birth weights of R857G Auxilin mice were also lower than their WT counterparts (Figure 1G). These results suggest that R857G Auxilin is a loss of function allele *in vivo* but that upregulation of the mutant variant occurs, allowing survival of mice carrying homozygous alleles.

Neurological phenotypes in R857G Auxilin mice phenocopy clinical features seen in patients

To assess neurological phenotypes in R857G Auxilin mice, we used a battery of behavioral tests on a longitudinal cohort of 8 mice per genotype at 6, 12 and 18 months of age. R857G Auxilin mice displayed balance impairments, as indicated by an increased tendency to fall from an elevated beam during the beam walk test compared to WT mice (Figure 2A; Figure S4A, Figure S5A). The pole test revealed progressive bradykinesia and decreased agility from 12 months onward in R857G Auxilin mice, as shown by an increased time to turn and to descend from a vertical wooden pole (Figure 2B, C; Figure S4B, C; Figure S5B, C). However, R857G Auxilin mice outperformed WT mice during the rotarod test, suggesting that the motor system is overall intact in these animals (Figure 2D; Figure S4D, Figure S5D). Analysis of the amplitude of movement over a broad-frequency range in a startle chamber revealed a decreased amplitude of movement in 12 month old R857G Auxilin mice (Figure 2E-G), which along with the pole test indicates bradykinesia. A subset of R857G Auxilin mice were observed to suffer seizures during cage changes (Video S1). Seizures were characterized by a freezing phenotype, followed by drooling and muscular twitching (Video S1). R857G Auxilin mice of up to 18 months of age were not observed to suffer from anxiety, memory, decreased forelimb strength or locomotor phenotypes, as assessed by the Y-maze, elevated plus maze, grip strength and open field tests (Figure S3). Taken together, these behavioral tests show R857G Auxilin mice develop neurological phenotypes that phenocopy clinical features seen in patients harboring mutations in Auxilin, including typical parkinsonian motor impairments, such as progressive bradykinesia and gait disturbances, as well as seizures. However, as many behaviors remain unaffected, the impairments are specific to a subset of motor functions.

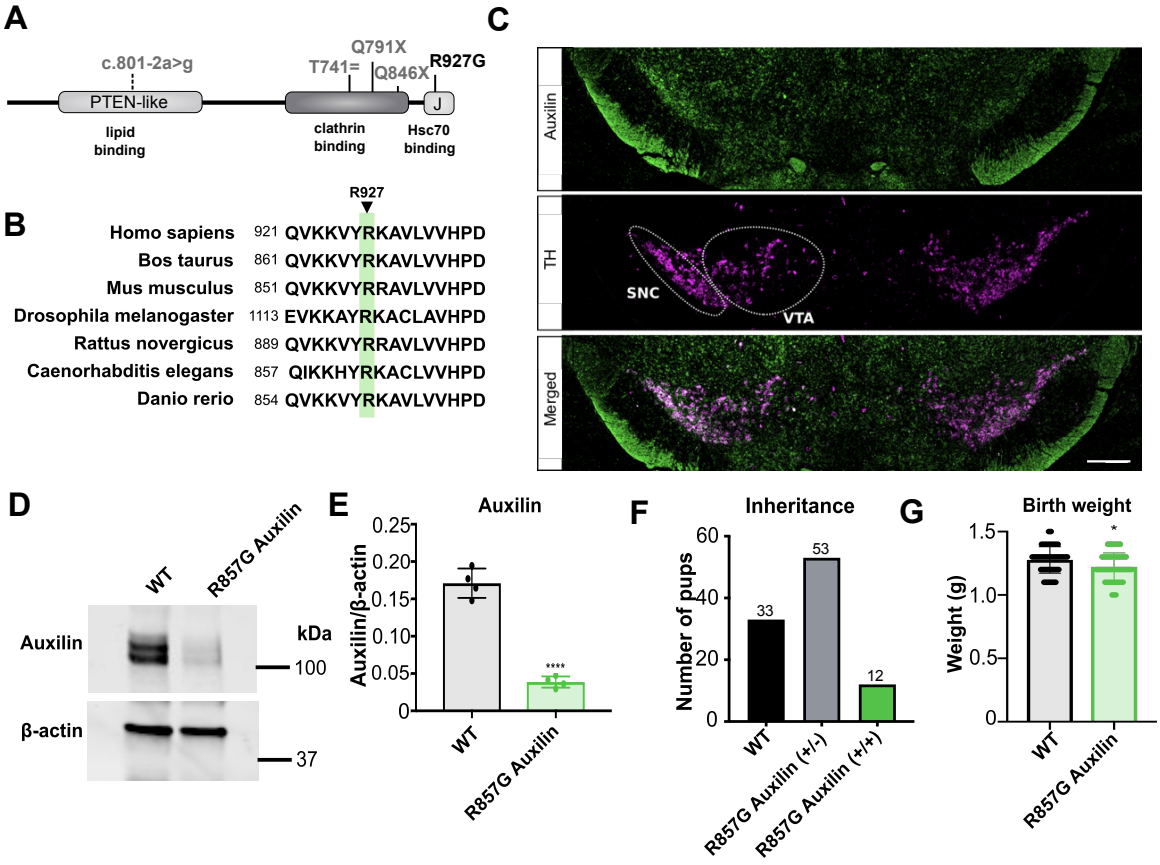

Figure 1. Novel PD mouse model with endogenous R857G Auxilin mutation displays hypomorphism during early development A Overview of Auxilin functional domains and pathogenic mutations. B The human R927 Auxilin residue is conserved across species and is equivalent to the murine R857 residue. C RNAscope of midbrain slices of 2 month old WT mice indicating Auxilin mRNA (green) and the dopaminergic neuronal marker TH mRNA (magenta). Scale bar indicates 800 μm. SNC substantia nigra pars compacta, VTA ventral tegmental area. E WB of primary neurons of WT and R857G Auxilin mice. F Quantification of normalized Auxilin levels of n = 4 independent cultures; ****, $p < 0.0001$ (unpaired, two-tailed Student's t-test with Welch's correction for unequal variance). G Survival bias of the offspring of heterozygous R857G Auxilin mating pairs at 3 weeks old n = 10 litters; $p < 0.01$ (χ-square test). H Body weight of newborn mice, n = 5 and n = 6 litters for WT and R857G Auxilin mice, respectively; * $p < 0.05$ (unpaired, two-tailed Student's t-test with Welch's correction for unequal variance).

Impaired synaptic recycling and dystrophic Golgi morphology in R857G Auxilin mice

PD is typically characterized by loss of dopaminergic (DA) neurons in the nigrostriatal pathway. Immunohistochemical analysis of tyrosine hydroxylase, a DA marker, did not reveal alterations in the substantia nigra or striatum of R857G Auxilin mice up to 12 months of age (Figure S6). The observed parkinsonian manifestations in R857G Auxilin mice are, therefore, not likely to be the result of gross dopaminergic neurodegeneration.

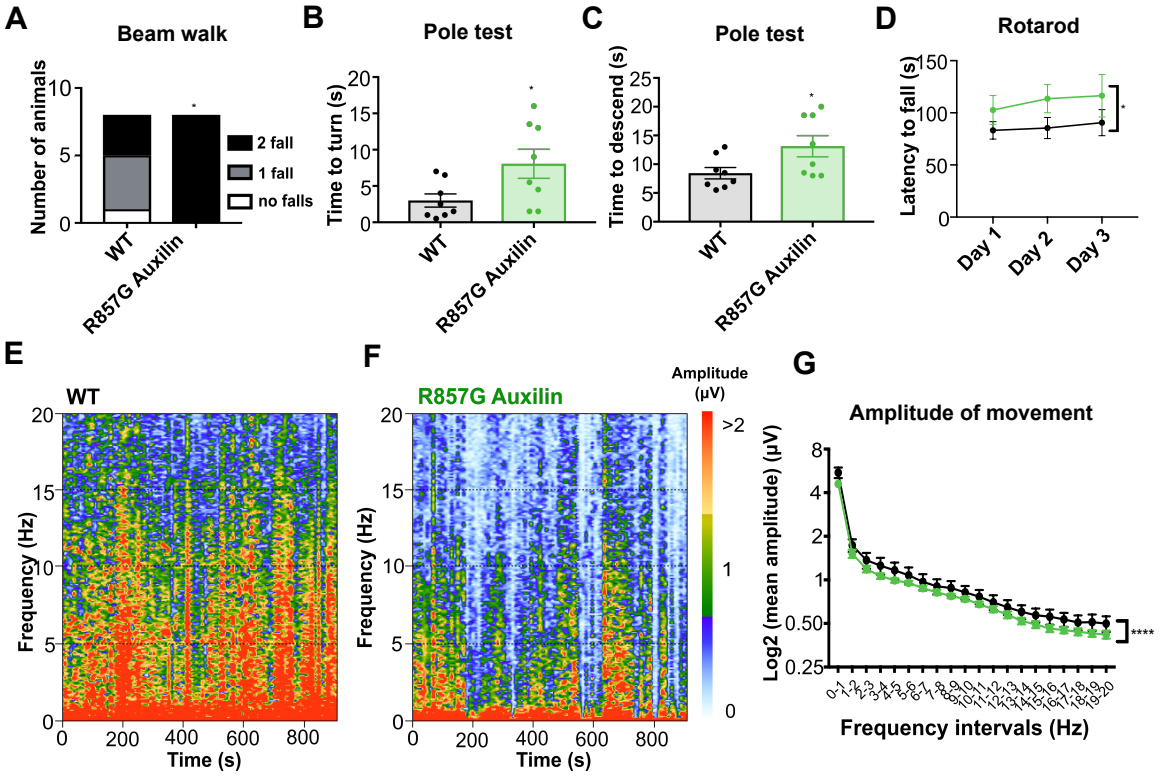

Figure 2. Motor impairments in 1 year old R857G Auxilin mice phenocopy clinical features observed in patients A Beam walk analysis indicating the number of falls when traversing a 6 mm beam during 2 trials; * $p < 0.05$ (χ-square test). B, C Performance during the pole test as analyzed by time to turn and time to descent; * $p < 0.05$ (unpaired, two-tailed Student's t-test with Welch's correction for unequal variance). D Latency to fall during the rotarod test during 3 consecutive days; $F(1, 42) = 4$;* $p < 0.05$ (Two-way ANOVA). E, F Analysis of the amplitude of movement in a startle chamber. Representative spectrographs of WT and R857G Auxilin mice are shown, displaying the amplitude (indicated by color) of movement during 15 minutes over a frequency range of 0-20 Hz. G Average mplitude of movement over a frequency range of 0-20 Hz; $F(1, 280) = 17.92$; **** $p < 0.0001$ (Two-way ANOVA). n = 8 mice per genotype.

To investigate the molecular impact of the R857G Auxilin mutation on clathrin structures and synaptic function, the ultra-structural morphology of nerve terminals was studied in the mutant mouse brain using electron microscopy. Since neurological defects were observed in R857G Auxilin mice as early as 6 months, this analysis was carried out in the dorsal striatum of 6 month old mice. Whereas the synaptic area of neurons in striatal section was unaltered, the number of presynaptic vesicles (SVs) was found to be decreased in R857G Auxilin mice (Figure 3A-D). The overall decrease in number of SVs suggests that synaptic recycling is impaired in mutant Auxilin mice due to inefficient uncoating of CCVs, as has previously been observed in mice with disrupted clathrin-associated endocytic proteins including Auxilin, Synaptojanin 1 and Endophilin 1 [22–26].

Although only a modest increase in CCVs was observed in the nerve terminals of R857G mice (Figure 3E), a significant increase of coated structures around the Golgi apparatus was observed (Figure 4A, B). Further EM analysis of Golgi morphology in the dorsal striatum of R857G Auxilin

mice revealed dystrophic morphological alterations of the Golgi apparatus. Golgi stacks in R857G Auxilin mice often appeared more swollen as compared to WT controls (Figure 4A, C, D). To be able to differentiate between *cis*, medial and *trans*-Golgi stacks, murine primary neurons were stained for endogenous Golgi markers and analyzed with enhanced-resolution microscopy. Swollen Golgi morphology would result in an increased surface area, with subsequent decrease of co-localization between neighboring Golgi stacks. Consistent with the hypothesis of Golgi swelling, decreased co-localization between *cis* and medial Golgi stacks (GM130 and GLG1, respectively) and medial and *trans*-Golgi stacks (GLG1 and TGN38, respectively) was observed in primary neurons derived from R857G Auxilin mice compared to WT (Figure 4E, F, G). Although a direct role for Auxilin at the Golgi apparatus has not been reported to date, our findings indicate that mutant Auxilin impairs uncoating of CCVs both at the synapse and the Golgi apparatus.

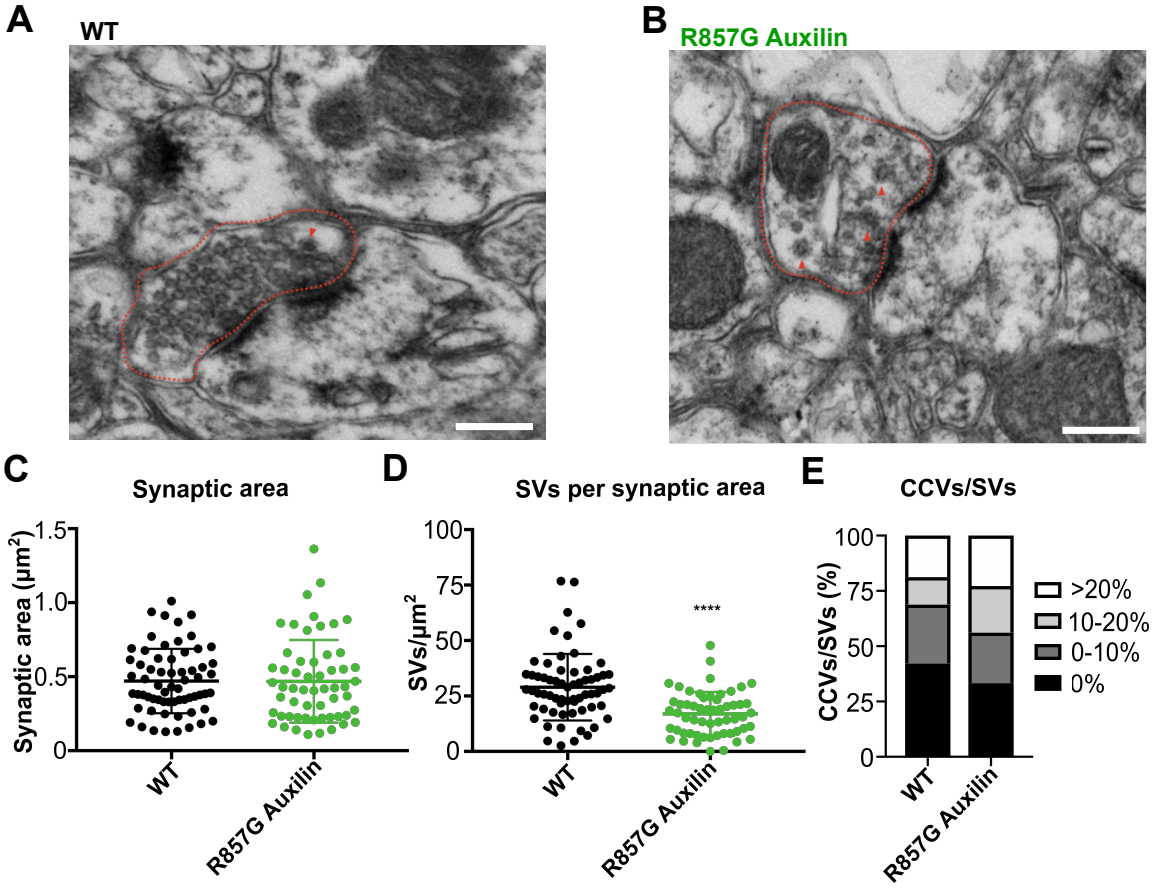

Figure 3. Impaired presynaptic vesicular recycling in R857G Auxilin mice A, B EM analysis of synaptic terminals in the striatum of WT and R857G Auxilin mice, respectively. Presynaptic areas are marked by red dotted lines and CCVs by red arrows. Scale bar indicates 300 nm. C Quantification of the presynaptic area. N = 64 and n = 57 synapses were analyzed for WT and R857G Auxilin mice, respectively. D Quantification of the number of synaptic vesicles per presynaptic area; **** p ¡ 0.0001 (unpaired, two-tailed Student's t-test with Welch's correction for unequal variance). E Quantification of the percentage of clathrin coated vesicles over synaptic vesicles.

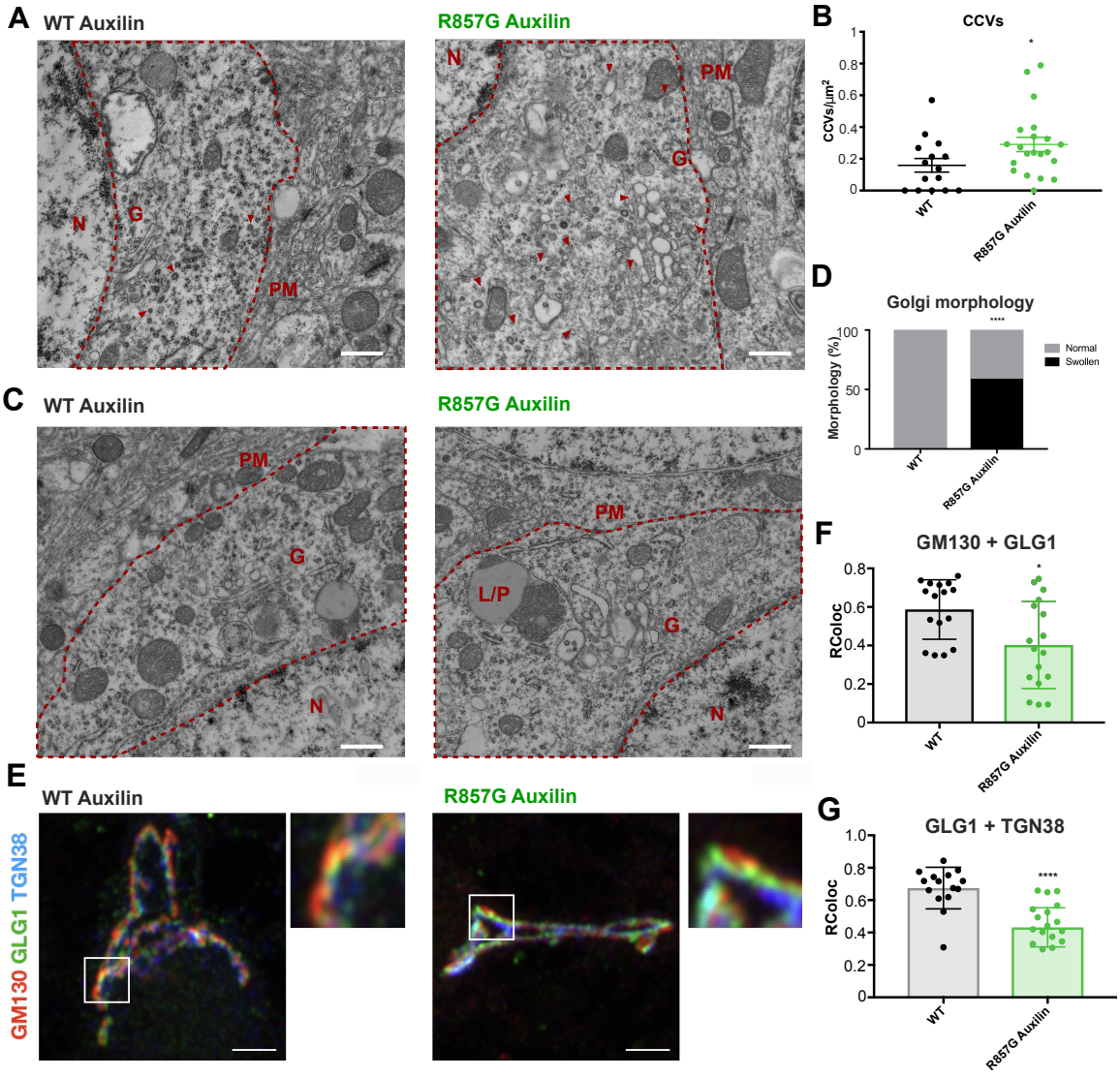

Figure 4. Accumulation of coated structures and dystrophic morphological alterations of the Golgi apparatus A, B Representative EM images of brain slices of the striatum of WT and R857G Auxilin mice. Scale bar = 600 nm. Neuronal cytoplasm is marked by red dotted lines. N = nucleus, G = Golgi, PM = plasma membrane. Red arrows indicate CCVs. B Quantification of the number of CCVs per cytoplasmic area, n = 15 and n = 21 cells analyzed for WT and R857G Auxilin mice, respectively; *, $p < 0.05$ (unpaired, two-tailed Student's t-test with Welch's correction for unequal variance). C, D Representative images of the striatum of WT and R857G Auxilin mice. Neuronal cytoplasm is marked by red dotted lines. Scale bar = 600 nm. PM = plasma membrane, N = nucleus, G = Golgi, L/P is lipid/protein inclusions. D Quantification of the observed Golgi morphologies of n = 10 and n = 22 WT and R857G Auxilin striatal cells, ****, $p < 0.0001$ (Binomial test). E Representative confocal images with Airyscan detection of WT and R857G Auxilin primary neurons, stained for endogenous GM130 (red), GLG1 (green) and TGN38 (blue). Scale bars = 2 μm. F, G Quantification of the co-localization of GLG1+GM130 and GLG1+TGN38 of n = 16 WT and n = 17 R857G Auxillin primary neurons; * $p < 0.05$, **** $p < 0.0001$ (unpaired, two-tailed Student's t-test with Welch's correction for unequal variance).

PD-like neuropathology in the striatum of R857G Auxilin mice

Efficient uncoating of Golgi-derived CCVs is a key event in the correct delivery of lysosomal proteins. Therefore, we hypothesized that impaired clathrin-mediated trafficking in R857G Auxilin mice may result in the accumulation of endolysosomal cargo in neurons. Remarkably, EM analysis revealed the presence of large intracellular lipid/proteinaceous aggregates reminiscent of lipofuscin in the dorsal striatum of R857G Auxilin mice (Figure 5A, Figure 4C). Progressive accumulation of lipofuscin has previously been observed in familial PD cases, pointing to impairments of the lysosomal system [2, 27]. To further assess the accumulation of cargo, midbrain sections were stained using BODIPY for neutral lipids in dopaminergic neurons in the substantia nigra. Neurons in R857G Auxilin mice contained less lipid droplets, but the size of each droplet was significantly increased, resulting in an overall increase of total lipid content per dopaminergic neuron in the SN of R857G Auxilin mice (Figure 5B-F).

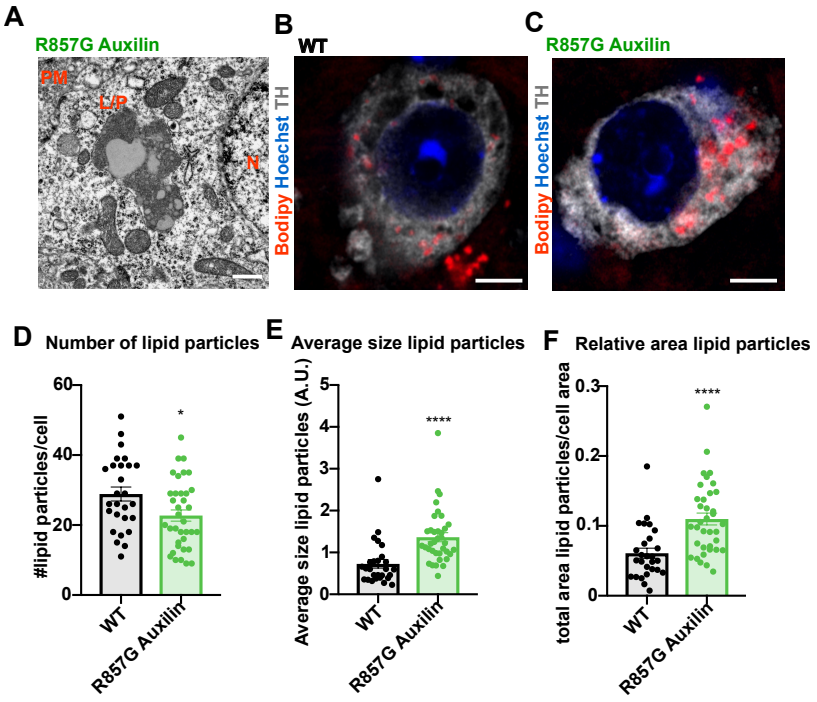

Figure 5. Accumulation of lipofuscin and lipids in neurons of R857G Auxilin mice A EM analysis of striatal sections of R857G Auxilin mice. PM, plasma membrane, L/P, lipid/protein inclusions, N, nucleus. Scale bar indicates 300 nm. B, C BODIPY staining and confocal imaging with Airyscan detection of DA neurons in sections of the SN of WT and R857G Auxilin mice. Scale bar indicates 5 μm. D, E, F Quantification of number of particles, particle size and lipid content per DA cell in the SN, respectively. 27 and 36 cells of n = 3 and n = 4 WT and R857G Auxilin mice, respectively, were analyzed; * $p < 0.05$, **** $p < 0.0001$ (unpaired, two-tailed Student's t-test with Welch's correction for unequal variance).

Auxilin interacts with clathrin adaptor proteins at the TGN and at the synapse

To gain further insight into a potential molecular function of Auxilin at the Golgi apparatus, the protein interactome of WT Auxilin was mapped in an unbiased fashion by combining GFP-nanotrap affinity purification with SILAC-based proteomics (Figure S7A). Experiments were performed in triplicate (figure S7B) and stringent bio-informatic filtering of protein interactors identified across all replicates resulted in a total of 32 top candidate Auxilin interactors (Figure 6A). Among the identified interactors were Auxilin itself and previously reported interactors clathrin heavy chain

(CLTC) and the plasma-membrane resident clathrin adaptor protein AP2 subunit α2 (AP2A2) [28], indicating that the experiment was successful in recovering authentic Auxilin interactors (Figure 6A). Gene ontology analysis of the top 32 candidate Auxilin interactors indicated an enrichment of clathrin-associated processes (Figure S7D) with both synaptic and Golgi apparatus-associated cellular components (Figure S7E). Of particular note, we identified the Golgi-resident clathrin adaptor protein GGA2 as a novel Auxilin interactor candidate.

To further compare and validate the interaction of Auxilin and its homologue GAK with multiple clathrin adaptor proteins, co-IPs were performed from HEK293FT cells transiently expressing GFP-Auxilin or GFP-GAK and WBs were probed for all endogenous adaptor proteins with a reported role in clathrin-mediated trafficking (AP1-3 and GGA1-3) (Figure 6B-G). We confirmed the interaction of Auxilin with AP2 and GAK with AP2 and AP1 as previously reported (Figure 6B, D, E) [15,16,28,29]. No interaction was observed between Auxilin or GAK with AP3 (Figure 6B). In addition, co-IP confirmed interaction between Auxilin and GGA2 and we also observed a weak interaction with GGA3, but not GGA1 (Figure 6C, F, G). GAK was not found to interact with any of the GGA proteins, as previously reported (Figure 6C, F, G) [15]. These data indicate that Auxilin and GAK both interact with the plasma membrane-resident AP2 but display differential binding with Golgi-resident clathrin adaptor proteins. In addition, this indicates for the first time a direct role for Auxilin in the uncoating of Golgi-derived CCVs. To test whether these interaction data are supported by spatial proximity within the cell using an alternative method, we transiently transfected GFP-Auxilin and examined co-localization with the TGN marker TGN38 (Figure 6K). The co-localization of Auxilin with this marker further supports a physiologically relevant function for Auxilin at the Golgi apparatus.

Identification of binding motifs required for differential interaction of Auxilin and GAK with Golgi-resident clathrin adaptor proteins

The γ-subunit of AP1 and the GGAs are γ-ear containing proteins that have previously been found to interact with accessory proteins through a conserved consensus motif ψG(P/D/E)(ψ/L/M) [30]. GAK interacts with AP1-γ via two sequences fitting this motif, namely FGPL and FGEF. These sequences are not conserved in Auxilin, which could explain its inability to interact with AP1 (Figure S8A). Further analysis of the Auxilin amino acid sequence revealed that Auxilin contains two sequences closely resembling the ψ(P/D/E)(ψ/L/M) consensus motif, namely FIPL (Figure S8B). Structural modelling of Auxilin and GGA2 shows the presence of the FIPL motifs on the surface of the tertiary structure and can be modelled to fit in close proximity with the basic surface residues of GGA2 required for recruitment of accessory proteins (Figure 6H). *In vitro* protein binding assay of 3x-Flag-Auxilin with GST-GGA2 showed a direct interaction between both proteins, making GGA2 a *bona fide* interactor of Auxilin. Mutagenesis of the putative GGA-binding motifs FIPL to AIPA (Figure S8C) markedly reduced interaction of Auxilin with GGA2, indicating that these motifs are indeed required for the interaction (Figure 6I, J). The FIPL motifs are not conserved in the GAK amino acid sequence, which may explain the inability of GAK to interact with GGA2 (Figure S8A).

Pathogenic Auxilin mutations impair interaction with clathrin

Next, we set out to address the impact of PD-associated mutations on the interactome of Auxilin. WT GFP-Auxilin or PD-associated coding mutants (Q791X, Q846X, R927G) were transiently expressed in cells and WB was performed on immunoprecipitated complexes for the presence of Auxilin interactors, namely clathrin heavy chain (CHC) and the clathrin adaptor proteins AP2, GGA2 and GGA3. Truncating mutations Q791X and Q846X, which lack some of the clathrin binding boxes (Figure S9A), resulted in a marked decrease of clathrin interaction (Figure 7A, E).

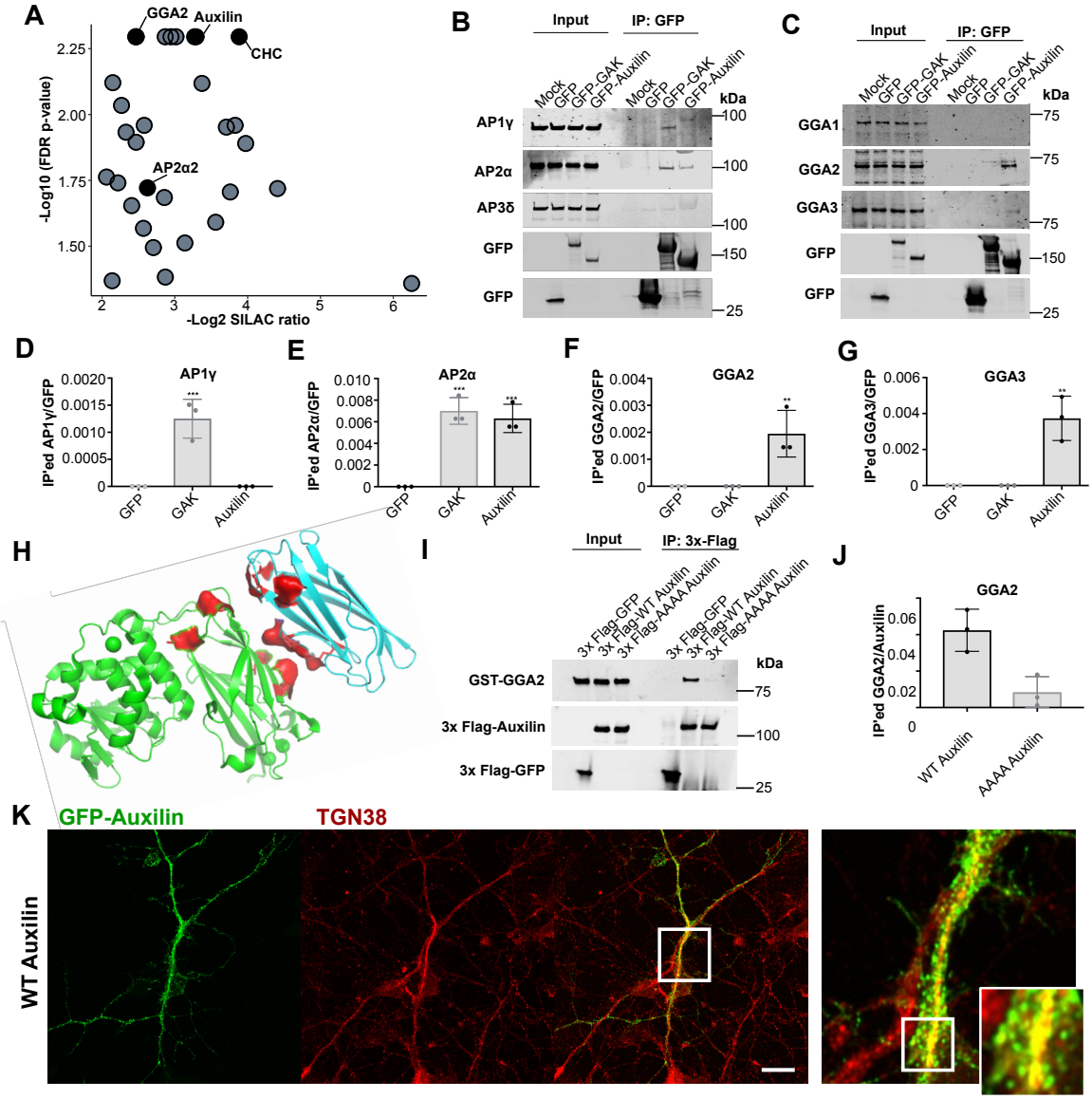

Figure 6. Auxilin interacts with a specific subset of synaptic and Golgi-resident clathrin adaptor proteins A Scatter plot of top candidate Auxilin interactors. B, C GFP-GAK or GFP-Auxilin were transiently expressed in HEK293FT cells and WB analysis was performed of GFP-nanotrap experiments for interaction with endogenous AP and GGA proteins. Images are representative of n = 3 replicates. D-G Quantification of AP1, AP2, GGA2, GGA3 interaction with GAK/Auxilin compared to GFP negative control and normalized to bait, n = 3; $F(2,6) = 36.42$, 41.37, 15.23, 27.57, respectively; with $p < 0.001$, ** $p < 0.01$ (One-way ANOVA with Tukey's post hoc test). H Modeling of Auxilin (green) with GGA2 (cyan). Interacting motifs are indicated in red (F and L from FIPL motifs in Auxilin, AR, K, RR from conserved surface motifs in GGA2 [31]). I Recombinant 3xFlag- GFP, 3xFlag-WT Auxilin or 3xFlag-AAAA Auxilin were incubated with recombinant GST-GGA2, followed by 3xFlag co-immunoprecipitation and WB analysis. Image is representative of n = 3 technical replicates. J Quantification of GGA2 co-purified with 3xFlag-Auxilin, normalized to bait; * , $p < 0.05$ (unpaired, two-tailed t-test). K Representative confocal images with Airyscan detection of murine primary neurons transiently transfected with GFP-Auxilin (green) and co-stained for the endogenous TGN marker TGN38 (red). Scale bar = 20 μm.

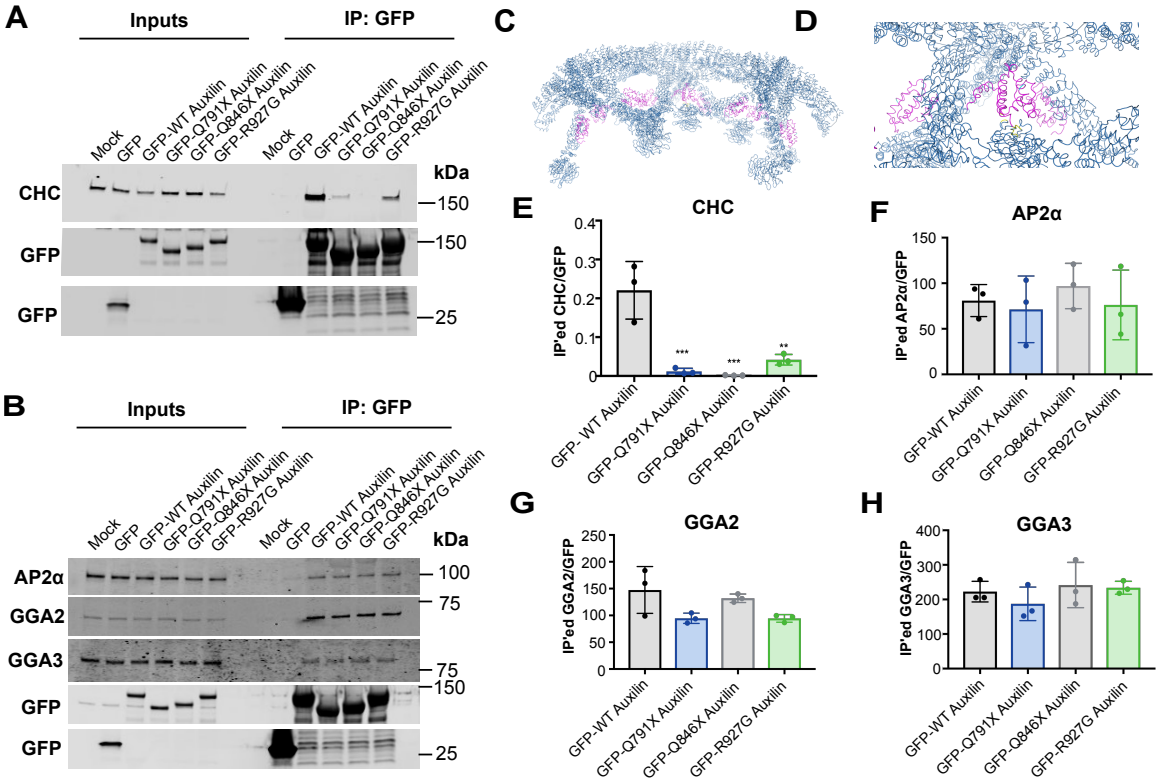

Figure 7. Impact of mutations on the interactome of Auxilin A, B GFP or WT, Q791X, Q846X, R927G Auxilin were transiently expressed in HEK293FT cells and WB analysis was performed on GFP-nanotrap experiments for interaction with endogenous CHC, AP2, GGA2 and GGA3. Images are representative of n = 3 replicates. C, D J-domain of bovine Auxilin (purple) bound to the assembled clathrin coat (dark blue) (PDB file derived from [10]). Auxilin residues residing at the interface with the clathrin coat (G825, P908, L909 and Y910, equivalent to human G885, P968, L969 and Y 970) are indicated in yellow. PD mutation (bovine R867, equivalent to human R927) is indicated in cyan.

Additionally, the point mutation R927G also impaired interaction of Auxilin with clathrin (Figure 7A, E). The R927G mutation resides within the J-domain of Auxilin (Figure S9A) [32, 33]; however, structural modelling of the J-domain with the clathrin coat shows that R927 is not in close proximity with the clathrin coat (Figure 6C, D). It is of note that the J-domain is composed of highly conserved α-helical structures, relying on the formation of hydrogen bonds between negatively and positively charged amino acids. Substitution of the positively charged R927 side chain to the uncharged and smaller G927 would therefore be likely to disrupt the tightly packed helical structure, resulting in a decreased ability of correct positioning within the assembled clathrin coat (Figure 7D). Even though the clathrin binding boxes appear the main determinants for clathrin interaction (Figure S10A) [16,28], additional low affinity interaction with the J-domain may further contribute to Auxilin interaction with the clathrin lattice. Interaction of the pathogenic Auxilin mutants with clathrin adaptor proteins AP2, GGA2 and GGA3 remained unaltered (Figure 7B, F-H). Despite the reduction of clathrin binding by pathogenic Auxilin mutants, transient expression of WT as well as mutant (Q791X, Q846X, R927G) GFP-Auxilin in primary neurons showed co-localization with endogenous

CCVs (Figure S8). This indicates that pathogenic Auxilin mutants can still be recruited correctly to CCVs, probably by interaction with the clathrin adaptors, but may be inefficient in the CCV uncoating reaction, as clathrin binding is crucial for the correct positioning of HSC70 for efficient clathrin uncoating. Therefore, the uncoating reaction will stall, resulting in a decreased turnover of CCVs as we have observed in mouse brain neurons (Figures 3 and 4). Collectively, these results define that mechanistically loss of function mutations in Auxilin result in loss of clathrin binding leading to a deficiency in vesicle uncoating and hence to neuronal dysfunction.

Discussion

Over the past two decades, a number of molecular pathways have been linked to the pathogenic events leading to neurodegeneration in PD, notably mitophagy and protein degradation pathways [2]. Here, we examined how disruption of the trafficking and delivery of CCVs by a mutation in the *DNAJC6* gene encoding Auxilin results in dopaminergic dysfunction and parkinsonism. By studying the loss of function mutations in Auxilin, we have also gained novel insights into its physiological activity and describe a novel role for Auxilin in the uncoating of Golgi-derived CCVs.

A role for Auxilin in the uncoating of CCVs at the synapse and the Golgi apparatus

Auxilin is the major neuronal CCV uncoating protein [8]. It is recruited to CCVs through membrane lipid interaction via its PTEN domain (Figure S9A) [34–36]. In addition, Auxilin interacts with the clathrin lattice via clathrin binding boxes and with HSC70 via its J-domain (Figure S9A) [11, 35–37]. The subsequent stimulation of the ATPase activity of HSC70 by Auxilin then acts to drive the uncoating of the clathrin coat [11–13, 38–40]. In addition to these key interactions, Auxilin has previously been found to interact with the plasma membrane-resident clathrin adaptor protein AP2 (Figure S9A) [15, 16, 28, 29], but not with the Golgi-resident AP1 [15]. Here, in addition to AP2, we identified GGA2, a Golgi-resident clathrin adaptor protein, as a novel *bona fide* Auxilin interactor (Figure 6, Figure S9A), thus describing for the first time a role for Auxilin in the uncoating of TGN-derived CCVs. Indeed, Auxilin was found to co-localize with the TGN (Figure 6K) and we observed an increase in coated vesicles both at the synapse and the Golgi apparatus in neurons with a missense mutation in Auxilin (Figures 3, 4A, B). In contrast, we find that the ubiquitously expressed homologue of Auxilin, GAK, interacts with AP1 and AP2, but not the GGA proteins (Figure 6) [15]. These results show that Auxilin and GAK interact with different Golgi-resident clathrin adaptors and suggest that the two homologues are partially redundant functionally.

Auxilin-associated mutations are loss of function mutations

Multiple recessive mutations in Auxilin have been associated with parkinsonism (Figure S9A). Two splice-site mutations (c.801-2A>G, T741=) are predicted to result in overall decreased expression of Auxilin and are thus hypomorphic [3, 5]. In addition, two C-terminally truncating mutations (Q791X, Q846X) completely lack the J-domain, required for interaction with HSC70, thus pointing to a partial loss of function mechanism [6, 7]. However, the mechanism of action of the R927G point mutation in the J-domain of Auxilin is less clear [5]. We engineered a novel mouse model carrying an R857G substitution in Auxilin, homologous to the R927G mutation in patients, and found that the R857G Auxilin allele is hypomorphic during early development, as demonstrated by decreased Auxilin protein levels in the brain of neonatal mice (Figure 1E, F; Figure S2). Structural modeling of Auxilin indicated that the R927G mutation resides within the coiled-coil J-domain,

thereby disrupting hydrogen bonds required for alpha-helical formation (Figure 7C, D). In addition, all nonsense (Q791X, Q846X) and missense (R927G) Auxilin mutations were found to disrupt or weaken the interaction with clathrin (Figure 7A, E). Interaction of Auxilin with clathrin is important for the correct positioning of HSC70 in close proximity to a subset of critical interactions within the clathrin lattice for the uncoating reaction [11]. It is thus conceivable that impaired clathrin interaction as well as disruption of the J-domain would impair CCV uncoating in Auxilin mutation carriers, resulting in the observed increased number of CCVs in the brain of R857G Auxilin mice (Figures 3, 4A, B).

Neuropathological lesions underlie PD-like neurological phenotypes in R857G Auxilin mice

We observed age-dependent movement phenotypes in R857G Auxilin mice, including bradykinesia and gait disturbances, as well as seizures (Figure 2, Video S1), similar to those observed in patients. These symptoms occurred in the absence of gross neurodegeneration (Figure S6), but were accompanied by pathological changes in the brain, including intracellular lipofuscin-like accumulations in the nigrostriatal pathways of R857G Auxilin mice (Figure 4 and 5). Impaired clathrin uncoating of TGN-derived CCVs results in impaired delivery of its cargo, including proteins and lipids, to their intracellular destination compartments (Figure 4 and 5). TGN-derived CCVs are particularly important for the delivery of hydrolases to the lysosomes [41]. Inefficient delivery of those hydrolases would therefore decrease the neuronal degradative capacity and further aggravate the accumulation of intracellular cargo (Figure 4 and 5), as has previously been reported for Auxilin depleted cells [42–47]. Clathrin-mediated trafficking also plays a major role in the recycling of synaptic vesicles [48]. Impaired clathrin uncoating of synaptic CCVs results in inefficient recycling of SVs, indicated by the decreased number of pre-synaptic SVs as observed in the brain of R857G Auxilin mice (Figure 3). Taken together, impaired clathrin-mediated trafficking in dopaminergic neurons, both at the synapse and the Golgi apparatus, may underlie the parkinsonism phenotypes, including progressive bradykinesia and gait disturbances, observed in R857G Auxilin mice (Figure S9B). In addition, impaired uncoating of CCVs in other brain areas might contribute to the epileptic seizures.

Clathrin-mediated trafficking and Parkinson's disease

In addition to Auxilin mutations, loss of function mutations in clathrin uncoating protein Synaptojanin 1 have also been associated with early onset PD. Patients with recessive mutations in the neuronal phosphatase synaptojanin 1, required for the shedding of clathrin adaptor proteins during CCV uncoating, present with similar phenotypes as described in Auxilin mutation carriers, including motor impairments and seizures [49]. These findings underscore an important role for clathrin coat dynamics in early onset PD and broaden the spectrum of pathways and cellular processes linked to dopaminergic dysfunction in the mammalian brain, further emphasizing the importance of intracellular vesicle trafficking. In this study, we describe a novel role for Auxilin in the uncoating of TGN-derived clathrin vesicles. Impaired lysosomal clearance and post-Golgi trafficking have previously been associated with PD pathogenesis, as multiple Mendelian genes including *LRRK2* and *VPS35* play prominent roles in vesicular trafficking between the Golgi apparatus and endosomes [21, 50]. In addition, multiple PD risk factors, including *GBA* and *CTSB*, are lysosomal hydrolases and require clathrin-mediated trafficking for their correct delivery to lysosomes [19, 20]. At a time when there is an urgent unmet need for disease modifying therapies for Parkinson's disease, our results further diversify the range of potential targets to be investigated and exploited. Response to L-DOPA, the first-line treatment in PD, is either absent or limited due to severe side-effects in Auxilin mutation carriers [3, 5–7]. Further dissection of clathrin-dependent pathways in neurons is therefore of particular interest to find novel

potential therapeutic targets. The murine model with endogenous PD-associated Auxilin mutation described herein provides a valuable platform to carry out such investigations, as well as to screen for potential disease modifying drugs for Parkinson's.

Materials and Methods

R857G Auxilin mice

For the generation of the R857G Auxilin mice on a C57BL/6 background, CRISPR sgRNA (AAGTGAAGAAGGTGTACAGG) and oligonucleotides (GGAGACCAAATGGAAACCCGTGGG CATGGCGGATCTGGTGACGCCGGAGCAAGTGAAGAAGGTGTACGGCCGCGCTGTGCTA GTGGTGCACCCTGACAAGGTGGGTAGCACCTGCCCTGTCGTAGACTTGCCCGGTCCCT GTTTCAGTGTTC) for CRISPR editing were designed using the web-based Benchling software (https://benchling.com). sgRNAs were selected based on their proximity to the PAM sequence and based on maximal on-target and minimal off-target effects (score system as described in [51]). Mouse mating pairs were set up on the day before micro-injection. Fertilized eggs were harvested and microinjected with Cas9 mRNA (12.5 ng/μl), sgRNA (4 ng/μl) and donor oligonucleotides (100 ng/μl). Zygotes were cultured overnight in M16 medium at 37°C and 2-cell stage embryos were implanted into oviducts of pseudo-pregnant surrogate mothers. Two male mice born to the foster mothers with successful homozygous gene editing were bred with C57BL/6J mice to establish the R857G Auxilin knockin mouse line. Mice were crossbred for at least 2 generations. The mice were given access to food and water *ad libitum* and housed in a facility with 12 hour light/dark cycles. All experiments were conducted in strict accordance with the recommendations in the Guide for the Care and Use of Laboratory Animals of the National Institutes of Health and approved by the Animal Care and Use Committees of the US National Institute on Aging.

Behavioral analysis

All behavioural experiments were performed during the light cycle of the mice and all animals were handled for 2 minutes on each of 3 days prior to testing. The longitudinal cohort consisted of 8 WT and 8 R857G Auxilin mice that were age-matched, with 4 male and 4 female mice per genotype. Animals were subjected to behavioural tests at 2, 6, 12 and 18 months of age.

Beam walk Mice were placed on an elevated narrow square beam 100 cm in length with an enclosed dark platform at the end of the beam. Mice were trained on a beam of 12 mm in width for 3 consecutive trials on 3 consecutive days. On testing day, time to traverse a 12 mm or 6 mm beam was measured for two consecutive trials.

Rotarod Mice were trained on a rotating rod for 5 minutes at a constant speed of 4 rpm. Starting the next day, mice were tested for three consecutive days on an accelerating rod from 4-40 rpm over 5 minutes. Latency to fall was determined 3 times for each mouse at 20 minute intervals and the average latency to fall was measured for each mouse per day. Pole test Mice were placed head-upward on the top of a wooden dowel (1 cm diameter, 0.5 m height) and recorded by video as they descended. One pre-trial was performed followed by two test trials. Time to descend to the floor of the cage as well as time to turn head-downward was measured and averaged for the two test trials. Maximal score was assigned for mice that did not turn or climb from the pole for time to turn and time to descend, respectively.

Grip strength Mouse grip strength was measured using a digital grip strength gauge. The apparatus was connected to a wire grid of 8 by 8 cm. The mice were lifted by the tail to allow them to grasp the grid with their forelimbs. Mice were pulled backward gently by the tail until the grid was released. The peak full force in grams exerted by the mouse before losing grip was recorded. The mean of 5

consecutive trials was recorded for each mouse.

Open field Mice were allowed to habituate in the testing room under red light for at least an hour. Mice were then placed in a Flex field photobeam activity system with 25.4 x 47 cm dimensions consisting of 4 x 8 photobeams for 30 minutes. Activity was tracked by photobeam breaks in real time. Total activity count was measured as the arithmetic count of the total number of beam breaks, fine movement count as the number of single beam breaks and subtraction of the fine movement counts from total movement counts resulted in the ambulatory event count. Rearing counts indicated the arithmetic count of all beam breaks registered by a second level of photobeams. Path length was calculated based on the coordinates of the beam breaks. Activity in the center was calculated by breaks of photobeams 2-3 (out of 4 total horizontal beams) and photobeams 3-6 (out of 8 total vertical beams).

Amplitude of movement Mice were placed in an SR-Lab startle response system for 15 minutes, in a non-restrictive plexiglass cylinder (3.2 cm diameter) resting on the sensor platform within a sound- and light-proof box. A piezo-electric accelerometer was attached to the base of the sensor platform, thus converting mouse displacement and acceleration into a voltage measurement, which was digitized by the SR-Lab software. Voltages were measured every ms throughout the entire test. For analysis, voltage measurements as a function of time were Fourier transformed to extract frequency information using the 'seewave' and 'rgl' package for R. Elevated plus maze Mice were allowed to habituate to the dimly lit (100 lutz) room for an hour. Mice were then placed in an elevated plus-shaped maze, with each arm of the maze 38 cm in length and 10 cm in width. Two arms of the maze opposite to each other were enclosed with 15 cm high walls. The mice were placed in the center of the maze facing a closed arm and were allowed to explore the maze for 10 minutes. The number of arm entries, time spent in each arm and percentage of entries into the open arms was scored.

Spontaneous alternation Mice were placed in a symmetrical Y-maze consisting of 3 arms, each 40 cm long, 8 cm wide and enclosed by plexiglass walls that were 12 cm high. Mice were placed in the center of the maze and were allowed to explore all 3 arms of the maze freely for 8 minutes. Spontaneous alternation was defined as consecutive entries in 3 different arms divided by the number of possible alternations.

Forced alternation The forced alternation task was conducted in the same Y-maze as described above. The forced alternation task consisted of a 5 minute sample trial and a 5 minute retrieval trial, with a 90 minute inter-trial interval. During the sample trial, the mice were placed in the start arm and were allowed to explore 2 arms of the Y-maze, whilst the third arm was blocked. During the retrieval, this block was removed and the mouse was placed in the start arm and allowed to freely explore all 3 arms of the Y-maze. Forced alternation was scored as the percentage of mice in the retrieval trial entering the arm that was blocked during the sample trial first. In addition, time spent in the novel arm was measured.

RNAscope

RNAscope was performed as described in [52]. Probes were designed for Auxilin (target region 235-1177 of NM 001164583.1), GAK (target region 395-1305 of NM 153569.2) and the DA neuronal marker TH (target region 483-1603 of NM 009377.1).

Immunofluorescence

Primary neurons from cortex were prepared from postnatal day 0 pups and plated onto coverslips precoated with poly-D-lysine (Neuvitro) at $0.5x10^6$ cells/wells as described [53]. Primary cortical neurons transfected using Lipofectamine 2000 (Invitrogen), according to manufacturer's instructions.

2 μg plasmid was transfected for a 12 mm coverslip in a single well of a 24-well plate of primary neurons cultured 7 DIV. Culture media was replaced 4 hours after transfection and immunocytochemistry was performed 40 hours after transfection. Cells were fixed for 20 minutes in PBS containing 4% paraformaldehyde and 120 mM sucrose, followed by permeabilization for 15 minutes with 0.2% Triton diluted in PBS. Non-specific binding sites were blocked for 30 minutes with 3% FBS in PBS. Next, neurons were incubated at RT for 1 hour with primary antibodies diluted in PBS containing 1% FBS (CHC (Abcam, ab21679), GM130 (Abcam, ab169276), GLG1 (ThermoFisher Scientific, PA5-26838), TGN38 (Bio-Rad, ab10552)). Cells were washed 3 times with PBS. Cells were subsequently incubated with Alexa Fluor secondary antibodies (ThermoFisher Scientific) diluted in PBS buffer containing 1% FBS for 30 minutes, followed by 3 washes with PBS-CM buffer. All secondary antibodies were donkey host and used at 1:500 dilution. Coverslips were mounted on microscope slides using ProLong gold Antifade Mountant (ThermoFisher Scientific) and dried overnight at RT in the dark. Immunohistochemistry was performed on the brains of 12 month old mice, transcardially perfused with saline. Brains were fixed in 4% PFA for 48 hour and subsequently transferred to a 30% sucrose solution. Fixed brains were cut into coronal 30 μm sections and stored in antifreeze solution (0.5 M phosphate buffer, 30% glycerol, 30% ethylene glycol) at -20°C until further processing. Brain sections were transferred to 24-well plate and washed from antifreeze solution with PBS twice for 10 min. Sections that were stained against DAT were subjected to antigen retrieval prior to immunostaining. Section were placed into Citric buffer (10mM sodium citrate, 0.05% Tween 20, pH 6.0) for 30 min at 80°C and were rinsed again afterwards with PBS buffer. All sections were then incubated in PBS containing 10% NDS, 1% BSA and 0.3% Triton for 30 minutes. Following blocking, sections were incubated primary antibodies (DAT (Abcam, ab111468), TH (Pel-freeze Biologicals, P40101-150), VMAT (ImmunoStar, 20042)) in antibody solution (1% NDS, 1% BSA and 0.3% Triton in PBS) overnight at 4°C. The next day, sections were rinsed three times with PBS for 10 min and incubated with AlexaFluor labeled secondary antibody (1:500, Invitrogen, Donkey host) in antibody solution for 1 hour. For neutral lipid staining, sections were incubated in 20 μg/ml BODIPY493/503 (Invitrogen). Afterwards, sections were washed three times with PBS for 10 min, mounted on glass slides and mounted using Prolong Gold Antifade mounting media (Invitrogen).

Electron microscopy

Striatal brain slices were collected from 10 month old mice. Mice were transcardially perfused with saline for 2 minutes, followed by perfusion with fixation buffer for 5 minutes (2% formaldehyde, 2% glutaraldehyde in 150 mM sodium-cacodylate, buffered at pH 7.4). Brains were isolated and postfixed for 8 hours in fixation buffer. Next, brains were rinsed overnight in 150 mM sodium-cacodylate buffer without fixatives. The following day, 200 μm thick coronal brain sections were sliced using a vibratome. Striatal sections around the anterior commissure level were submitted for conventional transmission EM imaging. Specimens were rinsed in cacodylate buffer, postfixed with 1% OsO4 in the same buffer on ice, en bloc stained with 1% uranyl acetate, dehydrated in an ethanol series and embedded in EMbed 812 resin (Electron Microscopy Sciences). Thin sections were cut, stained with uranyl acetate and lead citrate, and viewed with a JEM-1200EX (JEOL) transmission electron microscope (accelerating voltage 80 keV) equipped with an AMT 6 megapixel digital camera (Advanced Microscopy Techniques).

Confocal laser scanning microscopy with Airyscan detection

Airyscan imaging was performed in enhanced-resolution mode on a Zeiss LSM 880 Airyscan microscope equipped with a 63X, 1.4 NA objective. Raw data were processed using Airyscan processing in 'auto strength' mode with Zen Black software version 2.3.

SILAC-based proteomics

HEK293FT cells were metabolically labeled in DMEM supplemented with dialyzed 10% FBS, supplemented with 12C6 L-Lysine-2HCl (Lys-0) and 12C6 L-Arginine-HCl (Arg-0) or 13C6 L-Lysine-2HCl (Lys-8) and 13C6 L-Arginine-Hcl (Arg-10) for the metabolic incorporation of 'light' and 'heavy' stable isotopes respectively (ThermoFisher Scientific). HEK293FT cells were grown in light or heavy SILAC media for at least 10 doublings, allowing for higher than 98% efficient incorporation of the light or heavy stable isotopes. HEK293FT cells labelled with 'light' or 'heavy' SILAC isotopes were transfected with GFP or GFP-Auxilin, respectively, using Lipofectamine 2000 according to manufacturer's instructions. Co-immunoprecipitations were performed as described below and the resulting triplicate samples were loaded on a polyacrylamide gel for electrophoresis and subsequently cut out from the gel and subjected to in-gel trypsin digestion, followed by liquid chromatography tandem mass spectrometry analysis (LC-MS/MS). The LC-MS/MS data were searched against the NCBI Human database and Mascot Distiller software was used to calculate the protein Light/Heavy ratios [54,55]. Functional enrichment analysis was performed for the 50 most significantly differentially expressed genes using Gene Ontology [56,57] for gene Ontology terms 'biological process' and 'cellular component'. Fischer exact test was performed for functional enrichment analysis with Bonferroni post hoc correction. An enrichment map was generated using the 'EnrichmentMap' Cytoscape plug-in.

Co-immunoprecipitation and WB analysis

HEK293FT cells were transfected with GFP/GFP-Auxilin plasmid using Lipofectamine 2000, as per manufacturer's instructions. Co-IPs were performed 24 hours after transfection. Cells were resuspended lysis buffer (20 mM Tris pH7.5, 10% glycerol, 1 mM EDTA, 150 mM NaCl, 0.3% Triton) supplemented with 1x protease inhibitor cocktail and 1x phosphatase inhibitor cocktail (Halt) and rotated at 4°C for 30 minutes. Protein lysates were cleared by centrifugation for 10' at 4°C at 21,000 g). 1% input samples were prepared by dilution in 1x Laemmli sample buffer and boiling for 5 minutes at 95°C. For co-IPs, equal amounts of protein lysates were mixed with GFP-Trap agarose beads (Chromotek) and rotated at 4°C for one hour. Beads were subsequently washed 5 times with lysis buffer and boiled for 5 minutes at 95°C in 1X Laemmli sample buffer.

Western blot

Brain hemispheres were homogenized in lysis buffer (20 mM Tris pH7.5, 10% glycerol, 1 mM EDTA, 150 mM NaCl, 1x protease inhibitor cocktail (Halt), 1x phosphatase inhibitor cocktail (Halt)) with 1% Triton using glass homogenizers and samples were lysed on ice for 20min. Protein lysates were subsequently cleared (10' centrifugation at 4°C at 21 kg). Protein lysates were diluted to obtain final sample concentration of 30 μg per sample and boiled in 1x Laemmli Sample buffer (Bio-Rad). Protein samples were loaded on pre-cast 4-20% TGX polyacrylamide gels (Criterion, Bio-Rad). Electrophoresis was performed in 1x pre-mixed electrophoresis buffer (10 mM Tris, 10 mM Tricine, 0.01% SDS, pH 8.3, diluted with water) using the Criterion Vertical Electrophoresis Cell (Bio-Rad). Following gel electrophoresis, samples were transferred to Western blots were transferred to 0.45 μm pore-size nitrocellulose membranes (Bio-Rad) using the Trans-Blot Turbo Transfer System (Bio-Rad). Blocking of membranes was performed in a 1:1 solution of phosphate buffered saline (PBS) and Odyssey Blocking Buffer (Li-Cor). After blocking, membranes were incubated with primary antibodies diluted in antibody buffer (1:1 of Tris buffered saline (TBS) with 0.1% Tween and Odyss Blocking Buffer (Li-Cor)) overnight with gentle agitation at 4°C. Primary antibodies used for WB analysis were Auxilin (Novus Biologicals, NBP1-81507), GAK (Gift from Dr. Lois Greene), CHC (Abcam, ab21679), AP2 (Abcam, ab2730), AP1 (B & D Biosciences, 610385), GGA1 (Abcam, ab10551), GGA2 (Abcam, ab10552), GGA3 (B & D Biosciences, 612311), GFP (Sigma,

ab290), GST (Sigma, 27-4577-01), Flag (Sigma, F1804). Following primary antibody incubation, membranes were washed 3 times for 5 minutes in TBS-0.1% Tween. Membranes were then incubated with fluorescent secondary antibodies (IRDye, Li-Cor) diluted 1:15000 in antibody buffer for 1 hour at room temperature (RT) under gentle agitation. Secondary antibody incubation was followed by 3 washes of 5' each in TBS-0.1% Tween. Western blots were imaged using the Odyssey CLx system (Li-Cor) and quantified using Image Studio software.

Structural modeling

Structural models were generated using PyMOL (Version 2.0, Schrodinger, LLC). Modeling of the interaction between the Clathrin triskelion and the J-domain of Auxilin was performed utilizing the structure from Bos Taurus (PDB:1XI5) emphasizing the pathogenic mutation and interaction domain [11]. Representational modeling of potential interaction between GGA2 and Auxilin was performed using the previously solved structures (PDB: 3N0A-Auxilin and the S. cerevisiae GGA2 PDB: 3MNM) and based on predicted interaction sites [15, 31, 34, 58]. I-TASSER was utilized to predict the structure of human Auxilin and the strongest match was selected. The generated model was based on the Auxilin structure from Bos taurus (PDB: 3N0A) [34, 59–61]. Heterodimeric complex (Hsc70 and Auxilin) was modelled in PyMol overlaying the J-domain of the generated model with the Hsc70-J-domain structure available in the Protein Data Bank (PDB: 2QWO) [62].

Supporting Information

Supplementary video (available online)

Video S1: Seizure in R857G Auxilin mice Seizure observed in a 6 month old female R857G Auxilin mice. Seizing mice displayed muscle twitches at a frequency about 1.5 Hz, followed by a freezing phenotype and drooling.

Supplementary figures

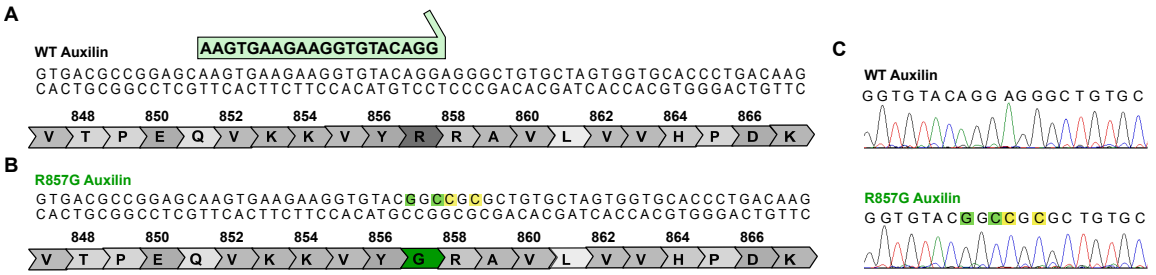

Figure S1. CRISPR design of R857G Auxilin mouse A, B Design of the R857G Auxilin mutant mouse at the level of amino acids and nucleotides with indication of the sgRNA sequence utilized for CRISPR editing. Silent mutations introduced to prevent additional CRISPR editing are indicated in yellow, missense mutations are indicated in green. C Sanger sequencing confirmed correct knockin of the R857G Auxilin mutation into the mouse genome.

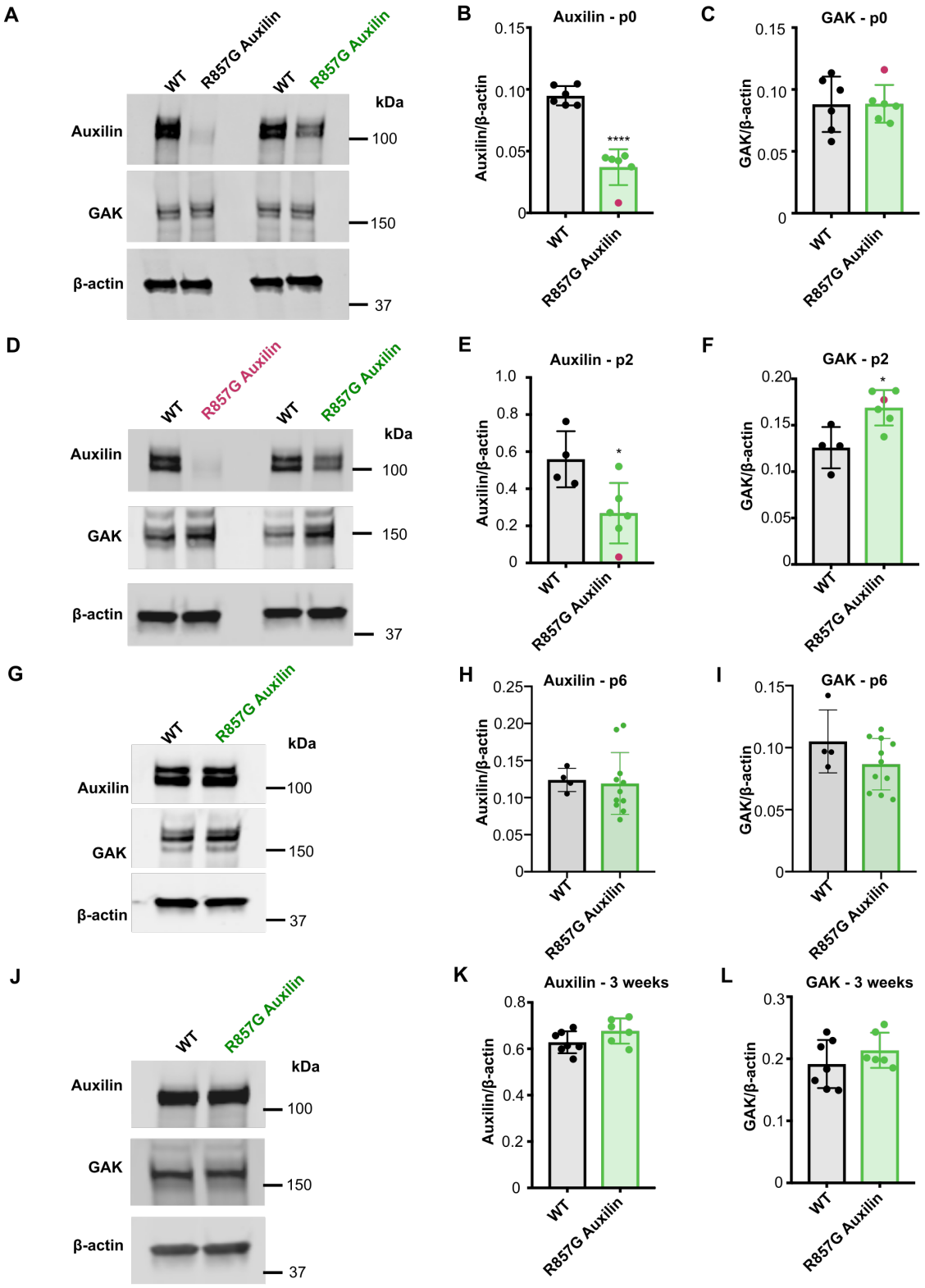

Figure S2. Alterations in Auxilin and GAK protein levels in the brain of R857G Auxilin mice (caption on next page)

Figure S2. Alterations in Auxilin and GAK protein levels in the brain of R857G Auxilin mice A, D, G, J WB of Auxilin and GAK in brain lysates of P0, P2, P6 and 3 week old mice, respectively. n = 4-6 per genotype. B, C, E, F, H, I, K, L Quantification of normalized Auxilin and GAK levels in the brain lysates of WT and R857G Auxilin mice; *, $p < 0.05$, **** $p < 0.0001$ (unpaired, two-tailed Student's t-test with Welch's correction for unequal variance).

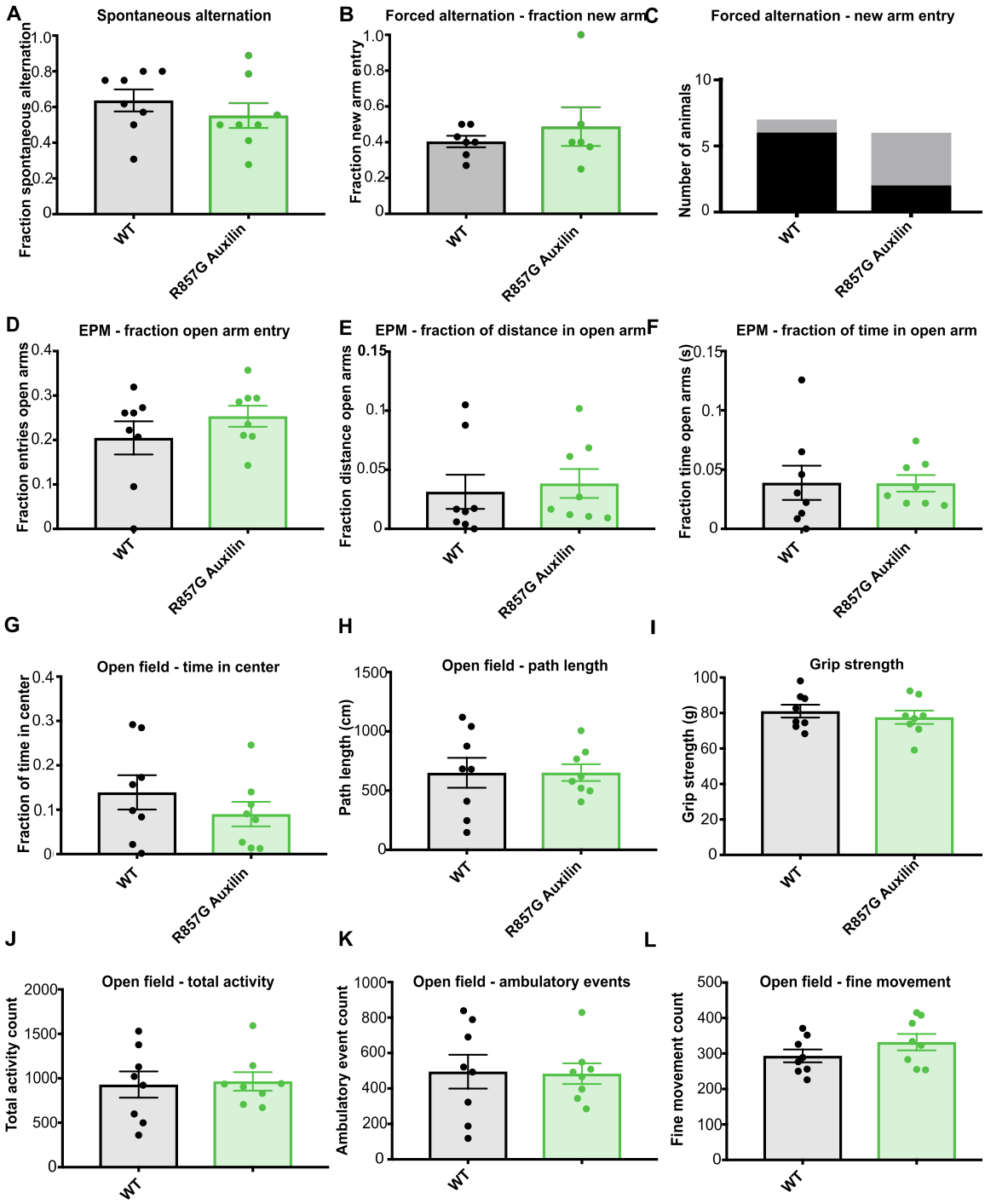

Figure S3. Anxiety, memory and locomotor phenotypes in 1 year old R857G Auxilin mice (Caption on next page)

Figure S3. Anxiety, memory and locomotor phenotypes in 1 year old R857G Auxilin mice A Y-maze spontaneous alternation test indicating the fraction of spontaneous alternations. B Y-maze forced alternation test indicating the fraction of entries the new arm. C Y-maze forced alternation test indicating the number of entries into the new arm upon first arm entry. D, E, F Fraction of open arm entries, fraction of distance travel in open arm and fraction of time spent in open arm of the elevated plus maze, respectively. G Time spent in the center of the open field test. H Total path length in the open field test. I Average forelimb strength measured during 5 trials of the grip strength test. J, K, L total activity, ambulatory activity and fine movement counts, respectively, of WT and R857G Auxilin mice in the open field test. n = 8 mice per genotype.

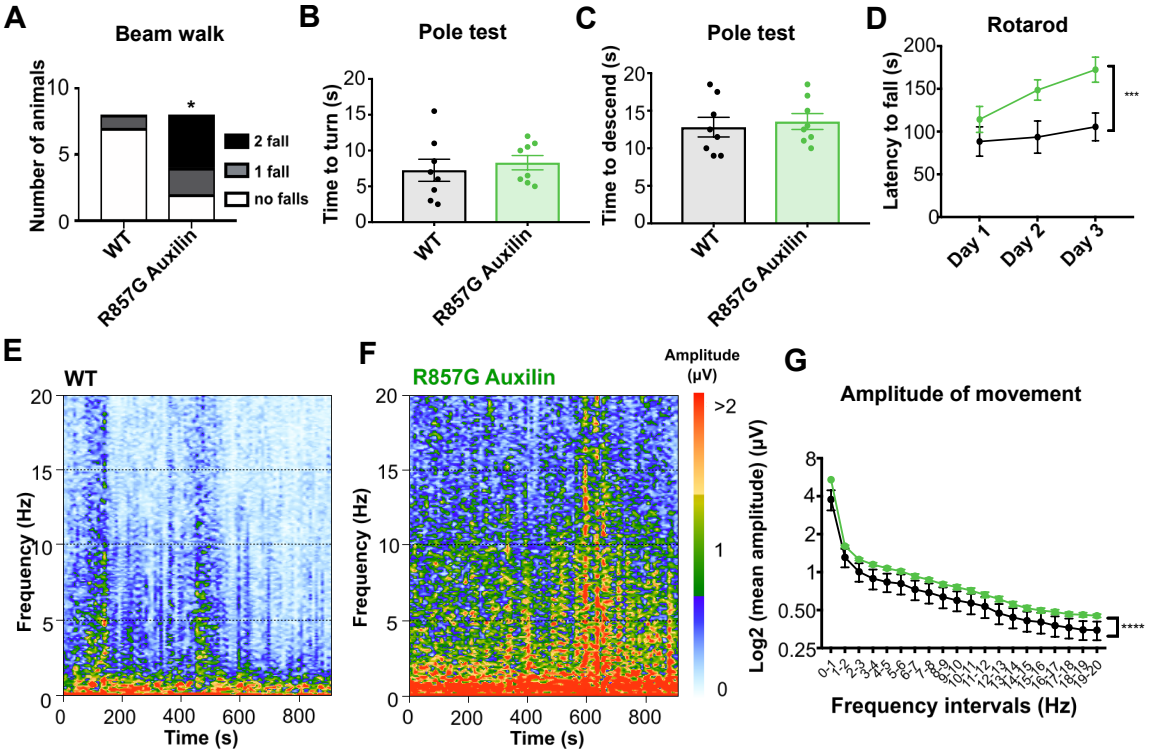

Figure S4. Motor impairments in 6 month old R857G Auxilin mice A Beam walk analysis indicating the number of falls when traversing a 6 mm beam during 2 trials;* $p < 0.05$ (χ-Square test). B, C Performance during the pole test as analyzed by time to turn and time to descent. D Latency to fall during the rotarod test during 3 consecutive days; $F(1,42) = 14.57$; *** $p < 0.001$ (Two-way ANOVA). E, F Analysis of the amplitude of movement in a startle chamber. Representative spectrograms of WT and R857G Auxilin mice are shown, displaying the amplitude (indicated by color) of movement during 15 minutes over a frequency range of 0-20 Hz. G Average amplitude of movement over a frequency range from 0-20 Hz; $F(1, 280) = 29.04$; ****, $p < 0.0001$ (two-way ANOVA). n = 8 mice per genotype.

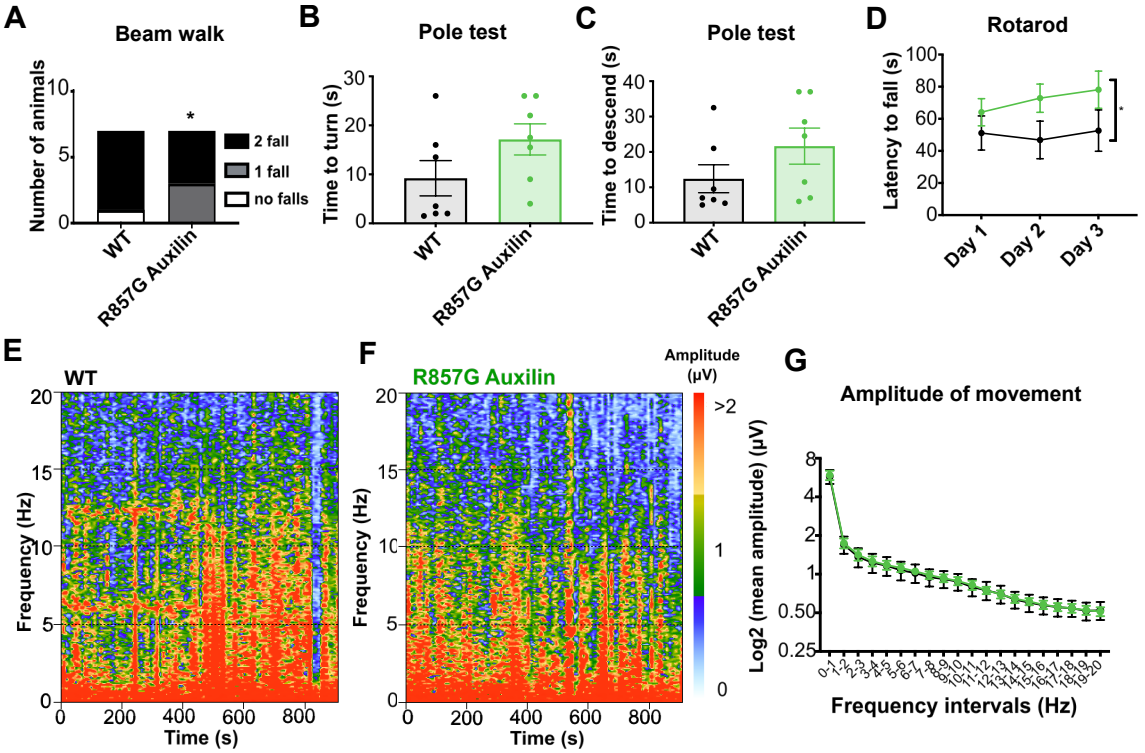

Figure S5. Motor impairments in 18 month old R857G Auxilin mice A Beam walk analysis indicating the number of falls when traversing a 6 mm beam during 2 trials. χ-square tests were performed; *, $p < 0.05$. B, C Performance during the pole test as analyzed by time to turn and time to descent. D Latency to fall during the rotarod test during 3 consecutive days; $F(1, 36) = 5.952$, * $p < 0.05$ E, F Analysis of the amplitude of movement in a startle chamber. Representative spectrograms of WT and R857G Auxilin mice are shown, displaying the amplitude (indicated by color) of movement during 15 minutes over a frequency range of 0-20 Hz. G Average amplitude of movement over a frequency range from 0-20Hz. n = 8 mice per genotype.

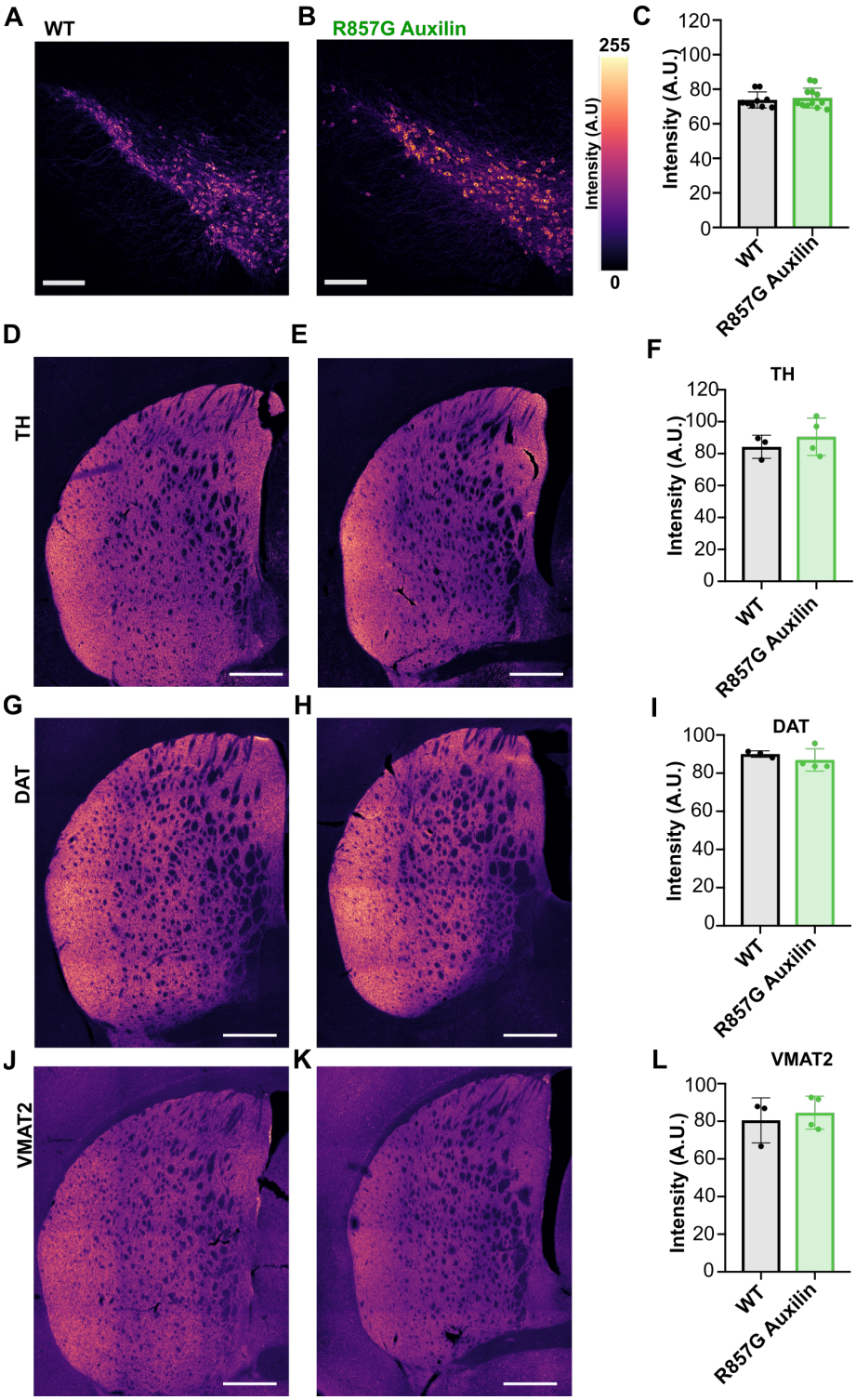

Figure S6. No dopaminergic neurodegeneration in 12 month old R857G Auxilin mice
(Caption on next page)

Figure S6. No dopaminergic neurodegeneration in 12 month old R857G Auxilin mice Staining for TH in the SN of WT and R857G Auxilin mice (A, B). Representative images are shown of 3 sections of n = 3 WT and n = 4 R857G Auxilin mice. Scale bar indicates 200 μm. Staining for TH (D, E), DAT (G, H) and VMAT2 (J,K) in the striatum of WT and R857G Auxilin mice. Representative images are shown of n = 3 and n = 4 WT and R857G Auxilin mice, respectively. Scale bar indicates 500 μm. Fluorescence intensity (F, I, L) was quantified and no significant differences were noted between genotypes (unpaired, two-tailed Student's t-test with Welch's correction for unequal variance).

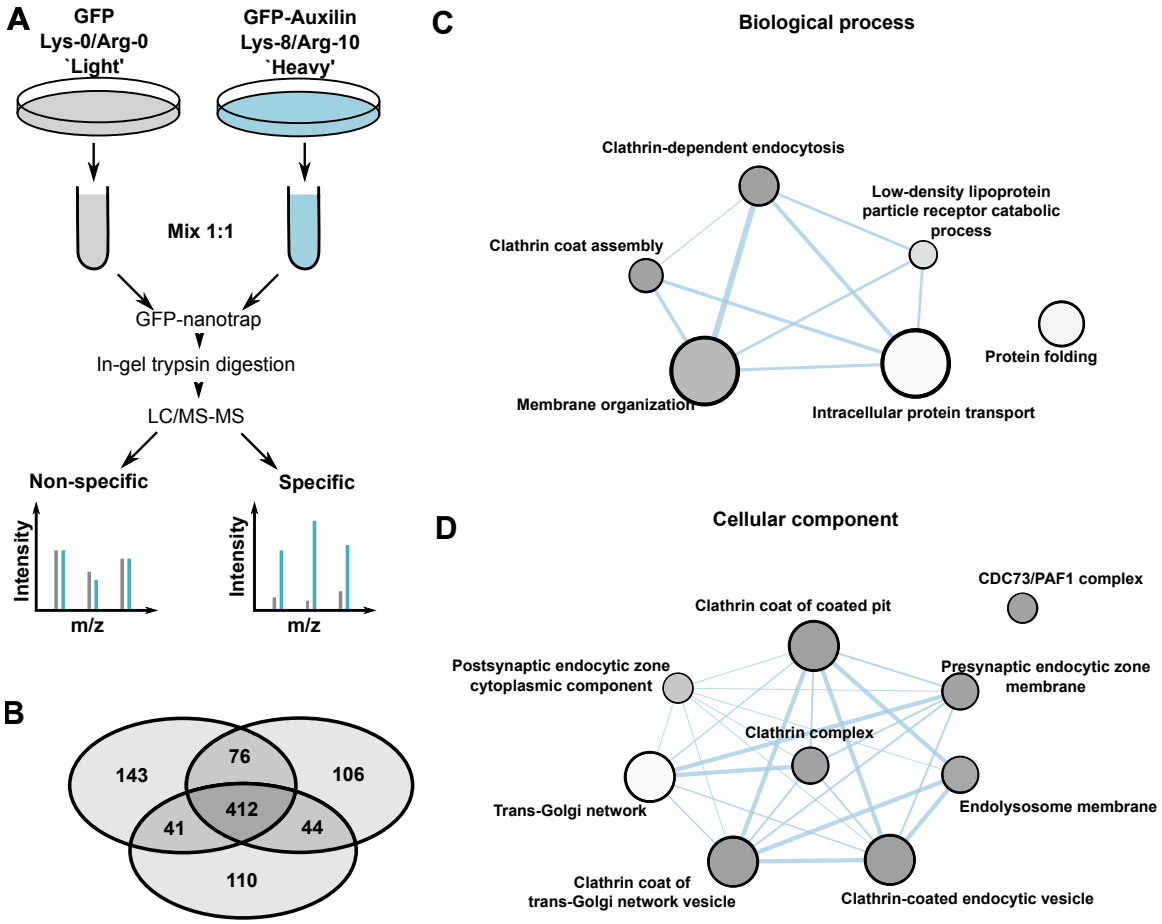

Figure S7. SILAC set-up and gene ontology analysis of the Auxilin interactome A Design of SILAC-based AP-MS approach to identify the interactome of Auxilin. HEK293FT cells were labelled with 'light' or 'heavy' amino acid epitopes and transfected with GFP or GFP-Auxilin, respectively. GF nanotrap co-IP was performed and precipitates were mixed 1:1, followed by in-gel trypsin digestion, LC-MS/ MS and subsequent protein identification. B Venn diagram of the number of proteins identified across 3 technical replicates of the SILAC experiment. C, D Gene ontology enrichment analysis of the top candidates of Auxilin interactors for biological process and cellular component. Node size corresponds to the number of proteins within each protein set and edge size to the number of overlapping proteins between connected nodes (larger is more proteins). Node color corresponds to the p-value of the Fisher exact test with Bonferroni correction for multiple testing (darker is lower p-value).

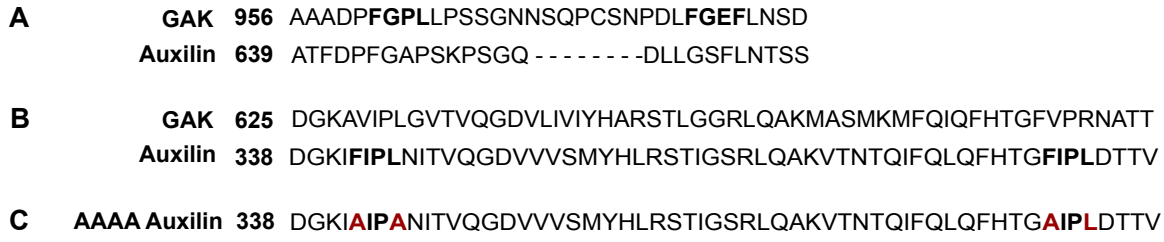

Figure S8. Interaction motifs for γ-ear containing accessory proteins in GAK and Auxilin A Binding motifs in GAK for AP1 binding are indicated in bold and are not conserved in Auxilin [15, 63]. B Putative binding motifs in Auxilin for GGA2 are indicated in bold and are not conserved in GAK [64]. C Mutation of putative GGA2 binding motifs in Auxilin, with mutated residues indicated in red.

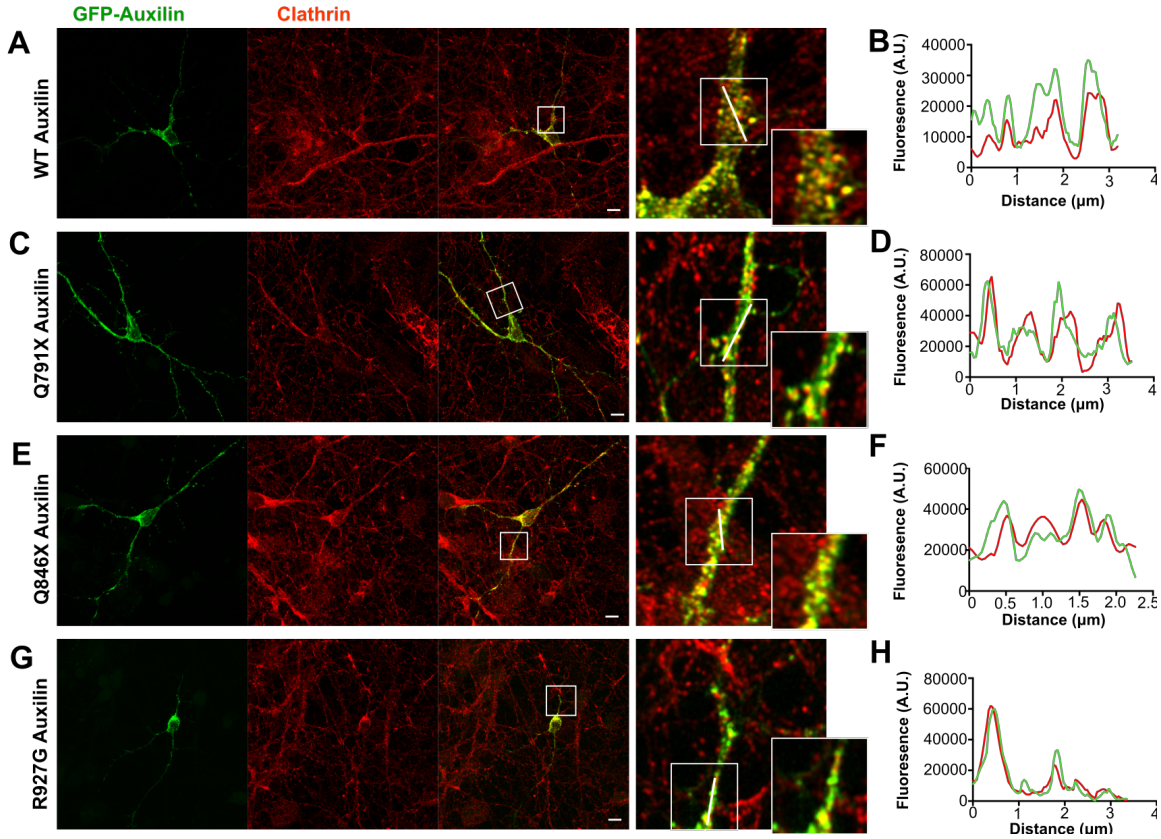

Figure S9. Co-localization of Auxilin with clathrin Representative confocal images with Airyscan detection of murine primary neurons transiently transfected with GFP-WT, Q791X, Q846X or R927G Auxilin (green) and co-stained for endogenous clathrin heavy chain (red). Scale bar = 20 μm. The right panel shows the fluorescence intensity profiles in function of the distance indicated in the magnified merged image. Scale bar = 2 μm.

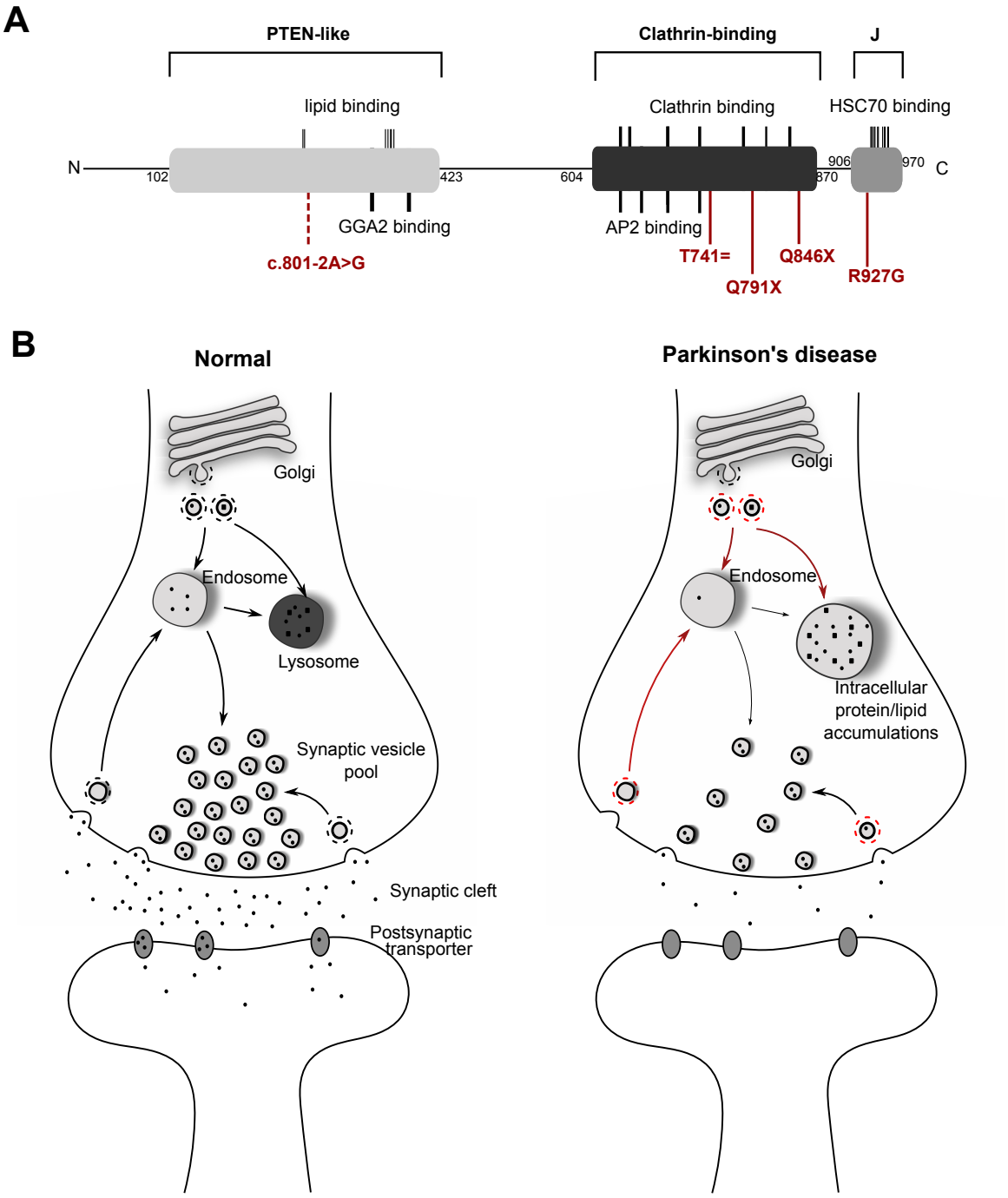

Figure S10. M Overview of *bona fide* Auxilin interactors and proposed model for disease pathogenesis in Auxilin mutation carriers A domain organization of Auxilin with indication of interaction motifs and residues involved with interaction for lipid, clathrin, HSC70, GGA2 and AP2 binding. Thickness of lines misrepresentative for number of residues involved with the interaction. Pathogenic mutations are shown in red, with solid line indicating coding variants and dotted line indicating exonic variant. B Model for PD pathogenesis in Auxilin mutation carriers Clathrin-mediated trafficking in neurons of normal population and PD patients. Impaired clathrin-mediated trafficking due to PD-associated Auxilin mutations would result in inefficient synaptic vesicle recycling, with subsequent decrease in number of vesicles in the presynaptic intracellular synaptic vesicle pool. In addition, inefficient clathrin-mediated trafficking from the TGN would result in impaired delivery of lysosomal hydrolases and therefore impair lysosomal maturation, resulting in an accumulation of intracellular cargo.

Acknowledgments

This research was supported in part by the Intramural Research Program of the NIH, National Institute on Aging and by the NIMH IRP Rodent Behavioral Core (ZIC MH002952 and MH002952 to Yogita Chudasama). DAR was supported by a University of Reading Graduate School Doctoral award. PAL is supported by MRC programme grant MR/N026004/1.

Author contributions

DAR, PAL and MRC conceptualized the research. CL generated the CRISPR KI mice. Structural models were generated by NS. YL performed mass-spectrometry analysis. CKEB performed electron microscopy. CDW, DCG and JSB contributed to enhanced-resolution light microscopy. NL performed immunohistochemistry experiments. MC, JDH and JD contributed to execution and analysis of behavioral experiments. SSA performed RNAscope experiments. AB, RK and AK contributed to primary neuronal culture experiments. LBP generated SILAC-labeled HEK293FT cells. DCG and LS contributed to the analysis of EM data. All other experiments were performed by DAR. DAR, PAL and MRC analyzed experiments and wrote the manuscript.

Declaration of interests

Authors declare no competing interests.

References

1. A. J. Lees, J. Hardy, and T. Revesz, "Parkinson's disease," *Lancet*, vol. 373, pp. 2055–2066, jun 2009.

2. R. Kumaran and M. R. Cookson, "Pathways to parkinsonism redux: convergent pathobiological mechanisms in genetics of Parkinson's disease," *Human Molecular Genetics*, vol. 9, pp. 1–37, 2015.

3. S. Edvardson, Y. Cinnamon, A. Ta-Shma, A. Shaag, Y. I. Yim, S. Zenvirt, C. Jalas, S. Lesage, A. Brice, A. Taraboulos, K. H. Kaestner, L. E. Greene, and O. Elpeleg, "A deleterious mutation in DNAJC6 encoding the neuronal-specific clathrin-uncoating co-chaperone auxilin, is associated with juvenile parkinsonism," *PLoS ONE*, vol. 7, no. 5, pp. 4–8, 2012.

4. J. Hardy, P. Lewis, T. Revesz, A. Lees, and C. Paisan-Ruiz, "The genetics of Parkinson's syndromes: a critical review," *Current Opinion in Genetics and Development*, vol. 19, pp. 254–265, 2009.

5. S. Olgiati, M. Quadri, M. Fang, J. P. M. A. Rood, J. A. Saute, H. F. Chien, C. G. Bouwkamp, J. Graafland, M. Minneboo, G. J. Breedveld, J. Zhang, International Parkinsonism Genetics Network, F. W. Verheijen, A. J. W. Boon, A. J. A. Kievit, L. B. Jardim, W. Mandemakers, E. R. Barbosa, C. R. M. Rieder, K. L. Leenders, J. Wang, and V. Bonifati, "DNAJC6 mutations associated with early-onset Parkinson's disease," *Annals of Neurology*, vol. 79, pp. 244–256, feb 2016.

6. L. E. O. Elsayed, V. Drouet, T. Usenko, I. N. Mohammed, A. A. A. Hamed, M. A. Elseed, M. A. Salih, M. E. Koko, A. Y. O. Mohamed, R. A. Siddig, M. I. Elbashir, M. E. Ibrahim,

A. Durr, G. Stevanin, S. Lesage, A. E. Ahmed, and A. Brice, "A novel nonsense mutation in DNAJC6 expands the phenotype of autosomal-recessive juvenile-onset Parkinson's disease," *Annals of Neurology*, vol. 79, pp. 335–337, feb 2016.

7. Ç. Köroglu, L. Baysal, M. Cetinkaya, H. Karasoy, and A. Tolun, "DNAJC6 is responsible for juvenile parkinsonism with phenotypic variability," *Parkinsonism and Related Disorders*, vol. 19, no. 3, pp. 320–324, 2013.

8. S. Ahle and E. Ungewickell, "Auxilin, a newly identified clathrin-associated protein in coated vesicles from bovine brain," *The Journal of Cell Biology*, vol. 111, pp. 19–29, jul 1990.

9. D.-W. Lee, X. Zhao, Y.-I. Yim, E. Eisenberg, and L. E. Greene, "Essential role of cyclin-G-associated kinase (Auxilin-2) in developing and mature mice," *Molecular Biology of the Cell*, vol. 19, pp. 2766–2776, jul 2008.

10. A. Fotin, Y. Cheng, N. Grigorieff, T. Walz, S. C. Harrison, and T. Kirchhausen, "Structure of an auxilin-bound clathrin coat and its implications for the mechanism of uncoating," *Nature*, vol. 432, pp. 649–653, dec 2004.

11. A. Fotin, Y. Cheng, P. Sliz, N. Grigorieff, S. C. Harrison, T. Kirchhausen, and T. Walz, "Molecular model for a complete clathrin lattice from electron cryomicroscopy," *Nature*, vol. 432, pp. 573–579, dec 2004.

12. I. Rapoport, W. Boll, A. Yu, T. Böcking, and T. Kirchhausen, "A Motif in the Clathrin Heavy Chain Required for the Hsc70/Auxilin Uncoating Reaction," *Molecular Biology of the Cell*, vol. 19, pp. 405–413, jan 2008.

13. E. Ungewickell, H. Ungewickell, and S. E. Holstein, "Functional interaction of the auxilin J domain with the nucleotide- and substrate-binding modules of Hsc70," *The Journal of Biological Chemistry*, vol. 272, pp. 19594–19600, aug 1997.

14. T. Greener, X. Zhao, H. Nojima, E. Eisenberg, and L. E. Greene, "Role of cyclin G-associated kinase in uncoating clathrin-coated vesicles from non-neuronal cells," *The Journal of Biological Chemistry*, vol. 275, pp. 1365–1370, jan 2000.

15. S. Kametaka, K. Moriyama, P. V. Burgos, E. Eisenberg, L. E. Greene, R. Mattera, and J. S. Bonifacino, "Canonical interaction of cyclin G associated kinase with adaptor protein 1 regulates lysosomal enzyme sorting," *Molecular Biology of the Cell*, vol. 18, pp. 2991–3001, aug 2007.

16. U. Scheele, C. Kalthoff, and E. Ungewickell, "Multiple interactions of auxilin 1 with clathrin and the AP-2 adaptor complex," *The Journal of Biological Chemistry*, vol. 276, pp. 36131–36138, sep 2001.

17. J. Lonsdale, J. Thomas, M. Salvatore, R. Phillips, E. Lo, S. Shad, R. Hasz, G. Walters, F. Garcia, N. Young, B. Foster, M. Moser, E. Karasik, B. Gillard, K. Ramsey, S. Sullivan, J. Bridge, H. Magazine, J. Syron, J. Fleming, L. Siminoff, H. Traino, M. Mosavel, L. Barker, S. Jewell, D. Rohrer, D. Maxim, D. Filkins, P. Harbach, E. Cortadillo, B. Berghuis, L. Turner, E. Hudson, K. Feenstra, L. Sobin, J. Robb, P. Branton, G. Korzeniewski, C. Shive, D. Tabor, L. Qi, K. Groch, S. Nampally, S. Buia, A. Zimmerman, A. Smith, R. Burges, K. Robinson, K. Valentino, D. Bradbury, M. Cosentino, N. Diaz-Mayoral, M. Kennedy, T. Engel, P. Williams, K. Erickson, K. Ardlie, W. Winckler, G. Getz, D. DeLuca, D. MacArthur, M. Kellis, A. Thomson, T. Young, E. Gelfand, M. Donovan, Y. Meng, G. Grant, D. Mash, Y. Marcus, M. Basile,

J. Liu, J. Zhu, Z. Tu, N. J. Cox, D. L. Nicolae, E. R. Gamazon, H. K. Im, A. Konkashbaev, J. Pritchard, M. Stevens, T. Flutre, X. Wen, E. T. Dermitzakis, T. Lappalainen, R. Guigo, J. Monlong, M. Sammeth, D. Koller, A. Battle, S. Mostafavi, M. McCarthy, M. Rivas, J. Maller, I. Rusyn, A. Nobel, F. Wright, A. Shabalin, M. Feolo, N. Sharopova, A. Sturcke, J. Paschal, J. M. Anderson, E. L. Wilder, L. K. Derr, E. D. Green, J. P. Struewing, G. Temple, S. Volpi, J. T. Boyer, E. J. Thomson, M. S. Guyer, C. Ng, A. Abdallah, D. Colantuoni, T. R. Insel, S. E. Koester, A. R. Little, P. K. Bender, T. Lehner, Y. Yao, C. C. Compton, J. B. Vaught, S. Sawyer, N. C. Lockhart, J. Demchok, and H. F. Moore, "The Genotype-Tissue Expression (GTEx) project," *Nature Genetics*, vol. 45, pp. 580–585, jun 2013.

18. Y. Zhang, S. A. Sloan, L. E. Clarke, C. Caneda, C. A. Plaza, P. D. Blumenthal, H. Vogel, G. K. Steinberg, M. S. B. Edwards, G. Li, J. A. Duncan, S. H. Cheshier, L. M. Shuer, E. F. Chang, G. A. Grant, M. G. H. Gephart, B. A. Barres, C. Agulhon, T. Fiacco, K. McCarthy, N. Allen, B. Barres, N. Allen, M. Bennett, L. Foo, G. Wang, C. Chakraborty, S. Smith, B. Barres, D. Attwell, A. Buchan, S. Charpak, M. Lauritzen, B. Macvicar, E. Newman, G. Banker, T. Beach, E. McGeer, K. Christopherson, E. Ullian, C. Stokes, C. Mullowney, J. Hell, A. Agah, J. Lawler, D. Mosher, P. Bornstein, B. Barres, W.-S. Chung, L. Clarke, G. Wang, B. Stafford, A. Sher, C. Chakraborty, J. Joung, L. Foo, A. Thompson, C. Chen, E. Al., W.-S. Chung, N. Allen, C. Eroglu, L. Clarke, B. Barres, F. Ding, J. O'Donnell, A. Thrane, D. Zeppenfeld, H. Kang, L. Xie, F. Wang, M. Nedergaard, L. Foo, N. Allen, E. Bushong, P. Ventura, W.-S. Chung, L. Zhou, J. Cahoy, R. Daneman, H. Zong, M. Ellisman, B. Barres, W.-P. Ge, A. Miyawaki, F. Gage, Y. Jan, L. Jan, D. Gordienko, T. Bolton, N. Hamilton, D. Attwell, X. Han, M. Chen, F. Wang, M. Windrem, S. Wang, S. Shanz, Q. Xu, N. Oberheim, L. Bekar, S. Betstadt, E. Al., M. Hawrylycz, E. Lein, A. Guillozet-Bongaarts, E. Shen, L. Ng, J. Miller, L. van de Lagemaat, K. Smith, A. Ebbert, Z. Riley, E. Al., P. Haydon, M. Nedergaard, W. Huang, B. Sherman, R. Lempicki, P. Huttenlocher, P. Huttenlocher, C. de Courten, L. Garey, H. V. der Loos, H. Kang, Y. Kawasawa, F. Cheng, Y. Zhu, X. Xu, M. Li, A. Sousa, M. Pletikos, K. Meyer, G. Sedmak, E. Al., B. Khakh, K. McCarthy, I. Kola, J. Landis, H. Kucukdereli, N. Allen, A. Lee, A. Feng, M. Ozlu, L. Conatser, C. Chakraborty, G. Workman, M. Weaver, E. Sage, E. Al., S. Kuffler, J. Nicholls, R. Orkand, N. Malik, X. Wang, S. Shah, A. Efthymiou, B. Yan, S. Heman-Ackah, M. Zhan, M. Rao, K. McCarthy, J. de Vellis, A. Meyer-Franke, M. Kaplan, F. Pfrieger, B. Barres, A. Molofsky, R. Krencik, E. Ullian, H.-H. Tsai, B. Deneen, W. Richardson, B. Barres, D. Rowitch, S. Mulligan, B. MacVicar, M. Nedergaard, A. Nimmerjahn, E. Mukamel, M. Schnitzer, N. Oberheim, X. Wang, S. Goldman, M. Nedergaard, N. Oberheim, T. Takano, X. Han, W. He, J. Lin, F. Wang, Q. Xu, J. Wyatt, W. Pilcher, J. Ojemann, E. Al., V. Parpura, T. Basarsky, F. Liu, K. Jeftinija, S. Jeftinija, P. Haydon, M. Paukert, A. Agarwal, J. Cha, V. Doze, J. Kang, D. Bergles, L. Pellerin, P. Magistretti, J. Rothstein, M. Dykes-Hoberg, C. Pardo, L. Bristol, L. Jin, R. Kuncl, Y. Kanai, M. Hediger, Y. Wang, J. Schielke, D. Welty, J. Schummers, H. Yu, M. Sur, W. Sun, E. McConnell, J. Pare, Q. Xu, M. Chen, W. Peng, D. Lovatt, X. Han, Y. Smith, M. Nedergaard, A. Tien, H. Tsai, A. Molofsky, M. McMahon, L. Foo, A. Kaul, J. Dougherty, N. Heintz, D. Gutmann, B. Barres, D. Rowitch, E. Ullian, S. Sapperstein, K. Christopherson, B. Barres, A. Winzeler, J. Wang, J. Zamanian, L. Xu, L. Foo, N. Nouri, L. Zhou, R. Giffard, B. Barres, Y. Zhang, K. Chen, S. Sloan, M. Bennett, A. Scholze, S. O'Keeffe, H. Phatnani, P. Guarnieri, C. Caneda, N. Ruderisch, E. Al., M. Zonta, M. Angulo, S. Gobbo, B. Rosengarten, K.-A. Hossmann, T. Pozzan, and G. Carmignoto, "Purification and Characterization of Progenitor and Mature Human Astrocytes Reveals Transcriptional and Functional Differences with Mouse," *Neuron*, vol. 89, pp. 37–53, jan 2016.

19. M. A. Nalls, N. Pankratz, C. M. Lill, C. B. Do, D. G. Hernandez, M. Saad, A. L. DeStefano,

E. Kara, J. Bras, M. Sharma, C. Schulte, M. F. Keller, S. Arepalli, C. Letson, C. Edsall, H. Stefansson, X. Liu, H. Pliner, J. H. Lee, R. Cheng, M. A. Ikram, J. P. A. Ioannidis, G. M. Hadjigeorgiou, J. C. Bis, M. Martinez, J. S. Perlmutter, A. Goate, K. Marder, B. Fiske, M. Sutherland, G. Xiromerisiou, R. H. Myers, L. N. Clark, K. Stefansson, J. A. Hardy, P. Heutink, H. Chen, N. W. Wood, H. Houlden, H. Payami, A. Brice, W. K. Scott, T. Gasser, L. Bertram, N. Eriksson, T. Foroud, and A. B. Singleton, "Large-scale meta-analysis of genome-wide association data identifies six new risk loci for Parkinson's disease," *Nature Genetics*, vol. 46, no. 9, pp. 989–993, 2014.

20. M. A. Nalls, C. Blauwendraat, C. L. Vallerga, K. Heilbron, S. Bandres-Ciga, D. Chang, M. Tan, D. A. Kia, A. J. Noyce, A. Xue, J. Bras, E. Young, R. von Coelln, J. Simon-Sanchez, C. Schulte, M. Sharma, L. Krohn, L. Pihlstrom, A. Siitonen, H. Iwaki, H. Leonard, F. Faghri, J. R. Gibbs, D. G. Hernandez, S. W. Scholz, J. A. Botia, M. Martinez, J.-C. Corvol, S. Lesage, J. Jankovic, L. M. Shulman, T. a. R. Team, S. G. o. P. D. S. Consortium, M. Sutherland, P. Tienari, K. Majamaa, M. Toft, A. Brice, J. Yang, Z. Gan-Orr, T. M. Gasser, P. M. Heutink, J. M. Shulman, N. A. Wood, D. A. Hinds, J. R. Hardy, H. R. Morris, J. M. Gratten, P. M. Visscher, R. R. Graham, A. B. Singleton, and I. P. D. G. Consortium, "Parkinson's disease genetics: identifying novel risk loci, providing causal insights and improving estimates of heritable risk," *bioRxiv*, aug 2018.

21. A. Beilina, I. N. Rudenko, A. Kaganovich, L. Civiero, H. Chau, S. K. Kalia, L. V. Kalia, E. Lobbestael, R. Chia, K. Ndukwe, J. Ding, M. a. Nalls, M. Olszewski, D. N. Hauser, R. Kumaran, A. M. Lozano, V. Baekelandt, L. E. Greene, J.-M. Taymans, E. Greggio, and M. R. Cookson, "Unbiased screen for interactors of leucine-rich repeat kinase 2 supports a common pathway for sporadic and familial Parkinson disease," *Proceedings of the National Academy of Sciences of the United States of America*, vol. 111, pp. 2626–2631, feb 2014.

22. Y.-I. Yim, T. Sun, L.-G. Wu, A. Raimondi, P. De Camilli, E. Eisenberg, and L. E. Greene, "Endocytosis and clathrin-uncoating defects at synapses of auxilin knockout mice," *Proceedings of the National Academy of Sciences of the United States of America*, vol. 107, pp. 4412–7, mar 2010.

23. O. Cremona, G. Di Paolo, M. R. Wenk, A. Lüthi, W. T. Kim, K. Takei, L. Daniell, Y. Nemoto, S. B. Shears, R. A. Flavell, D. A. McCormick, and P. De Camilli, "Essential Role of Phosphoinositide Metabolism in Synaptic Vesicle Recycling," *Cell*, vol. 99, pp. 179–188, oct 1999.

24. I. Milosevic, S. Giovedi, X. Lou, A. Raimondi, C. Collesi, H. Shen, S. Paradise, E. O'Toole, S. Ferguson, O. Cremona, and P. De Camilli, "Recruitment of endophilin to clathrin-coated pit necks is required for efficient vesicle uncoating after fission," *Neuron*, vol. 72, no. 4, pp. 587–601, 2011.

25. K. R. Schuske, J. E. Richmond, D. S. Matthies, W. S. Davis, S. Runz, D. A. Rube, A. M. Van Der Bliek, and E. M. Jorgensen, "Endophilin is required for synaptic vesicle endocytosis by localizing synaptojanin," *Neuron*, 2003.

26. P. Verstreken, T. W. Koh, K. L. Schulze, R. G. Zhai, P. R. Hiesinger, Y. Zhou, S. Q. Mehta, Y. Cao, J. Roos, and H. J. Bellen, "Synaptojanin is recruited by endophilin to promote synaptic vesicle uncoating," *Neuron*, 2003.

27. Y. Tong, E. Giaime, H. Yamaguchi, T. Ichimura, Y. Liu, H. Si, H. Cai, J. V. Bonventre, and J. Shen, "Loss of leucine-rich repeat kinase 2 causes age-dependent bi-phasic alterations of the autophagy pathway.," *Molecular neurodegeneration*, vol. 7, p. 2, jan 2012.

28. U. Scheele, J. Alves, R. Frank, M. Duwel, C. Kalthoff, and E. Ungewickell, "Molecular and functional characterization of clathrin- and AP-2-binding determinants within a disordered domain of auxilin," *The Journal of Biological Chemistry*, vol. 278, pp. 25357–25368, jul 2003.

29. D. J. Owen, Y. Vallis, M. E. Noble, J. B. Hunter, T. R. Dafforn, P. R. Evans, and H. T. McMahon, "A Structural Explanation for the Binding of Multiple Ligands by the α-Adaptin Appendage Domain," *Cell*, vol. 97, pp. 805–815, jun 1999.

30. R. Mattera, B. Ritter, S. S. Sidhu, P. S. McPherson, and J. S. Bonifacino, "Definition of the consensus motif recognized by gamma-adaptin ear domains," *The Journal of Biological Chemistryhemistry*, vol. 279, pp. 8018–8028, feb 2004.

31. T. Nogi, Y. Shiba, M. Kawasaki, T. Shiba, N. Matsugaki, N. Igarashi, M. Suzuki, R. Kato, H. Takatsu, K. Nakayama, and S. Wakatsuki, "Structural basis for the accessory protein recruitment by the γ-adaptin ear domain," *Nature Structural Biology*, vol. 9, p. 527, jun 2002.

32. J. M. Gruschus, C. J. Han, T. Greener, J. A. Ferretti, L. E. Greene, and E. Eisenberg, "Structure of the Functional Fragment of Auxilin Required for Catalytic Uncoating of Clathrin-Coated Vesicles," *Biochemistry*, vol. 43, no. 11, pp. 3111–3119, 2004.

33. J. Jiang, A. B. Taylor, K. Prasad, Y. Ishikawa-Brush, P. J. Hart, E. M. Lafer, and R. Sousa, "Structure Function Analysis of the Auxilin J-Domain Reveals an Extended Hsc70 Interaction Interface," *Biochemistry*, vol. 42, no. 19, pp. 5748–5753, 2003.

34. R. Guan, H. Dai, D. Han, S. C. Harrison, and T. Kirchhausen, "Structure of the PTEN-like region of auxilin, a detector of clathrin-coated vesicle budding," *Structure*, vol. 18, pp. 1191–1198, sep 2010.

35. D.-W. Lee, X. Wu, E. Eisenberg, and L. E. Greene, "Recruitment dynamics of GAK and auxilin to clathrin-coated pits during endocytosis," *Journal of Cell Science*, vol. 119, pp. 3502–3512, sep 2006.

36. R. H. Massol, W. Boll, A. M. Griffin, and T. Kirchhausen, "A burst of auxilin recruitment determines the onset of clathrin-coated vesicle uncoating," *Proceedings of the National Academy of Sciences of the United States of America*, vol. 103, pp. 10265–10270, jul 2006.

37. K. He, R. Marsland III, S. Upadhyayula, E. Song, S. Dang, B. R. Capraro, W. Wang, W. Skillern, R. Gaudin, M. Ma, and T. Kirchhausen, "Dynamics of phosphoinositide conversion in clathrin-mediated endocytic traffic," *Nature*, pp. 410–414, dec 2017.

38. S. E. Holstein, H. Ungewickell, and E. Ungewickell, "Mechanism of clathrin basket dissociation: separate functions of protein domains of the DnaJ homologue auxilin," *The Journal of Cell Biology*, vol. 135, pp. 925–937, nov 1996.

39. T. Böcking, F. Aguet, S. C. Harrison, and T. Kirchhausen, "Single-molecule analysis of a molecular disassemblase reveals the mechanism of Hsc70-driven clathrin uncoating," *Nature Structural & Molecular Biology*, vol. 18, pp. 295–301, mar 2011.

40. Y. Xing, T. Böcking, M. Wolf, N. Grigorieff, T. Kirchhausen, and S. C. Harrison, "Structure of clathrin coat with bound Hsc70 and auxilin: mechanism of Hsc70-facilitated disassembly," *The EMBO Journal*, vol. 29, pp. 655–665, feb 2010.

41. T. Braulke and J. S. Bonifacino, "Sorting of lysosomal proteins," *Biochimica et Biophysica Acta*, vol. 1793, pp. 605–614, apr 2009.

42. W. E. Gall, M. A. Higginbotham, C. Chen, M. F. Ingram, D. M. Cyr, and T. R. Graham, "The auxilin-like phosphoprotein Swa2p is required for clathrin function in yeast.," *Current biology : CB*, vol. 10, pp. 1349–58, nov 2000.

43. T. Greener, B. Grant, Y. Zhang, X. Wu, L. E. Greene, D. Hirsh, and E. Eisenberg, "Caenorhabditis elegans auxilin: a J-domain protein essential for clathrin-mediated endocytosis in vivo," *Nature Cell Biology*, vol. 3, pp. 215–219, feb 2001.

44. E. J. Hagedorn, J. L. Bayraktar, V. R. Kandachar, T. Bai, D. M. Englert, and H. C. Chang, "Drosophila melanogaster auxilin regulates the internalization of Delta to control activity of the Notch signaling pathway," *The Journal of Cell Biology*, vol. 173, pp. 443–452, may 2006.

45. J. Hirst, D. A. Sahlender, S. Li, N. B. Lubben, G. H. H. Borner, and M. S. Robinson, "Auxilin depletion causes self-assembly of clathrin into membraneless cages in vivo.," *Traffic (Copenhagen, Denmark)*, vol. 9, pp. 1354–71, aug 2008.

46. J. R. Morgan, K. Prasad, S. Jin, G. J. Augustine, and E. M. Lafer, "Uncoating of clathrin-coated vesicles in presynaptic terminals: roles for Hsc70 and auxilin.," *Neuron*, vol. 32, pp. 289–300, oct 2001.

47. B. Pishvaee, G. Costaguta, B. G. Yeung, S. Ryazantsev, T. Greener, L. E. Greene, E. Eisenberg, J. M. McCaffery, and G. S. Payne, "A yeast DNA J protein required for uncoating of clathrin-coated vesicles in vivo," *Nature Cell Biology*, vol. 2, pp. 958–963, dec 2000.

48. T. Soykan, T. Maritzen, and V. Haucke, "Modes and mechanisms of synaptic vesicle recycling," aug 2016.

49. M. Cao, Y. Wu, G. Ashrafi, M. H. Ellisman, T. A. Ryan, P. D. Camilli, M. Cao, Y. Wu, G. Ashrafi, A. J. Mccartney, H. Wheeler, E. A. Bushong, D. Boassa, M. H. Ellisman, T. A. Ryan, and P. D. Camilli, "Parkinson Sac Domain Mutation in Synaptojanin 1 Impairs Clathrin Uncoating at Synapses and Triggers Dystrophic Changes in Dopaminergic Axons Article Parkinson Sac Domain Mutation in Synaptojanin 1 Impairs Clathrin Uncoating at Synapses and Triggers Dystro," *Neuron*, vol. 93, no. 4, pp. 882–896, 2017.

50. E. Zavodszky, M. N. Seaman, K. Moreau, M. Jimenez-Sanchez, S. Y. Breusegem, M. E. Harbour, and D. C. Rubinsztein, "Mutation in VPS35 associated with Parkinson's disease impairs WASH complex association and inhibits autophagy," *Nature Communications*, vol. 5, dec 2014.

51. J. G. Doench, N. Fusi, M. Sullender, M. Hegde, E. W. Vaimberg, K. F. Donovan, I. Smith, Z. Tothova, C. Wilen, R. Orchard, H. W. Virgin, J. Listgarten, and D. E. Root, "Optimized sgRNA design to maximize activity and minimize off-target effects of CRISPR-Cas9," *Nature Biotechnology*, vol. 34, pp. 184–191, feb 2016.

52. F. Wang, J. Flanagan, N. Su, L.-C. Wang, S. Bui, A. Nielson, X. Wu, H.-T. Vo, X.-J. Ma, and Y. Luo, "RNAscope: A Novel in Situ RNA Analysis Platform for Formalin-Fixed, Paraffin-Embedded Tissues," *The Journal of Molecular Diagnostics*, vol. 14, pp. 22–29, jan 2012.

53. M. K. McCoy, A. Kaganovich, I. N. Rudenko, J. Ding, and M. R. Cookson, "Hexokinase activity is required for recruitment of parkin to depolarized mitochondria.," *Human molecular genetics*, vol. 23, pp. 145–56, jan 2014.

54. N. A. O'Leary, M. W. Wright, J. R. Brister, S. Ciufo, D. Haddad, R. McVeigh, B. Rajput, B. Robbertse, B. Smith-White, D. Ako-Adjei, A. Astashyn, A. Badretdin, Y. Bao, O. Blinkova, V. Brover, V. Chetvernin, J. Choi, E. Cox, O. Ermolaeva, C. M. Farrell, T. Goldfarb, T. Gupta, D. Haft, E. Hatcher, W. Hlavina, V. S. Joardar, V. K. Kodali, W. Li, D. Maglott, P. Masterson, K. M. McGarvey, M. R. Murphy, K. O'Neill, S. Pujar, S. H. Rangwala, D. Rausch, L. D. Riddick, C. Schoch, A. Shkeda, S. S. Storz, H. Sun, F. Thibaud-Nissen, I. Tolstoy, R. E. Tully, A. R. Vatsan, C. Wallin, D. Webb, W. Wu, M. J. Landrum, A. Kimchi, T. Tatusova, M. DiCuccio, P. Kitts, T. D. Murphy, and K. D. Pruitt, "Reference sequence (RefSeq) database at NCBI: current status, taxonomic expansion, and functional annotation," *Nucleic Acids Research*, vol. 44, pp. 733–745, jan 2016.

55. D. N. Perkins, D. J. C. Pappin, D. M. Creasy, and J. S. Cottrell, "Probability-based protein identification by searching sequence databases using mass spectrometry data," *Electrophoresis*, vol. 20, pp. 3551–3567, dec 1999.

56. The Gene Ontology Consortium, "The Gene Ontology Resource: 20 years and still GOing strong," *Nucleic Acids Research*, vol. 47, pp. D330–D338, jan 2019.

57. The Gene Ontology Consortium, M. Ashburner, C. A. Ball, J. A. Blake, D. Botstein, H. Butler, J. M. Cherry, A. P. Davis, K. Dolinski, S. S. Dwight, J. T. Eppig, M. A. Harris, D. P. Hill, L. Issel-Tarver, A. Kasarskis, S. Lewis, J. C. Matese, J. E. Richardson, M. Ringwald, G. M. Rubin, G. Sherlock, and G. Sherlock, "Gene ontology: tool for the unification of biology," *Nature Genetics*, vol. 25, pp. 25–9, may 2000.

58. P. Fang, X. Li, J. Wang, L. Niu, and M. Teng, "Structural Basis for the Specificity of the GAE Domain of yGGA2 for Its Accessory Proteins Ent3 and Ent5," *Biochemistry*, vol. 49, pp. 7949–7955, sep 2010.

59. A. Roy, A. Kucukural, and Y. Zhang, "I-TASSER: a unified platform for automated protein structure and function prediction," *Nature Protocols*, vol. 5, pp. 725–738, apr 2010.

60. J. Yang, R. Yan, A. Roy, D. Xu, J. Poisson, and Y. Zhang, "The I-TASSER Suite: protein structure and function prediction," *Nature Methods*, vol. 12, pp. 7–8, jan 2015.

61. Y. Zhang, "I-TASSER server for protein 3D structure prediction," *BMC Bioinformatics*, vol. 9, dec 2008.

62. J. Jiang, E. G. Maes, A. B. Taylor, L. Wang, A. P. Hinck, E. M. Lafer, and R. Sousa, "Structural Basis of J Cochaperone Binding and Regulation of Hsp70," *Molecular Cell*, vol. 28, pp. 422–433, nov 2007.

63. S. F. Altschul, W. Gish, W. Miller, E. W. Myers, and D. J. Lipman, "Basic local alignment search tool," *Journal of Molecular Biology*, vol. 215, pp. 403–410, oct 1990.

64. S. F. Altschul, T. L. Madden, A. A. Schäffer, J. Zhang, Z. Zhang, W. Miller, and D. J. Lipman, "Gapped BLAST and PSI-BLAST: a new generation of protein database search programs.," *Nucleic acids research*, vol. 25, pp. 3389–402, sep 1997.